AMERICAN METEOROLOGICAL SOCIETY

Journal of Physical Oceanography

EARLY ONLINE RELEASE

This is a preliminary PDF of the author-produced manuscript that has been peer-reviewed and accepted for publication. Since it is being posted so soon after acceptance, it has not yet been copyedited, formatted, or processed by AMS Publications. This preliminary version of the manuscript may be downloaded, distributed, and cited, but please be aware that there will be visual differences and possibly some content differences between this version and the final published version.

The DOI for this manuscript is doi: 10.1175/2008JPO3958.1

The final published version of this manuscript will replace the preliminary version at the above DOI once it is available.

© 2008 American Meteorological Society

AMERICAN METEOROLOGICAL SOCIETY 1919

Wave-driven circulation of a coastal reef-lagoon system

Ryan J. Lowe[1,2*], James L. Falter[3], Stephen G. Monismith[2] and Marlin J. Atkinson[3]

(1) School of Environmental Systems Engineering, University of Western Australia, Crawley, Australia

(2) Environmental Fluid Mechanics Laboratory, Stanford University, Stanford, CA

(3) Hawaii Institute of Marine Biology, University of Hawaii, Kaneohe, HI

Corresponding author: Ryan.Lowe@uwa.edu.au

PRELIMINARY ACCEPTED VERSION

Submitted to *Journal of Physical Oceanography* on 29 November 2007

First revision received on 5 May 2008; and in final form on 24 September 2008

AMERICAN METEOROLOGICAL SOCIETY 1919

Abstract

The response of the circulation of a coral reef system in Kaneohe Bay, Hawaii to incident wave forcing was investigated using field data collected during a ten-month experiment. Results from the study revealed that wave-forcing was the dominant mechanism driving the circulation over much of Kaneohe Bay. As predicted theoretically, wave setup generated near the reef crest due to wave breaking established a pressure gradient that drove flow over the reef and out the two reef channels. Maximum reef setup was found to be roughly proportional to the offshore wave energy flux above a threshold root-mean-squared wave height of 0.7 m (at which height setup was negligible). On the reef flat, the wave-driven currents increased approximately linearly with incident wave height; however, the magnitude of these currents were relatively weak (typically <20 cm/s) due to: 1) the mild fore-reef slope of Kaneohe Bay that reduced setup due to a combination of frictional wave damping and its relatively wide surfzone compared to steep-faced reefs; and 2) the presence of significant wave setup inside its coastally-bounded lagoon, due to frictional resistance on the lagoon-channel return flows, which reduced cross-reef setup gradients by 60-80%. In general, the dynamics of these wave-driven currents roughly matched predictions derived from quasi one-dimensional mass and momentum balances that incorporated radiation stresses, setup gradients, bottom friction and the morphological properties of the reef-lagoon system.

PRELIMINARY ACCEPTED VERSION

AMERICAN METEOROLOGICAL SOCIETY 1919

1 Introduction

Although winds, tides and buoyancy forcing can govern the circulation of some reefs, breaking waves have long been recognized as the dominant forcing mechanism on many reefs (Munk and Sargent 1954; Symonds et al. 1995; Kraines et al. 1998; Lugo-Fernandez et al. 2004; Callaghan et al. 2006). Conceptually, wave breaking increases the mean water level $\bar{\eta}$ in the surfzone ("wave setup"), establishing a pressure gradient that drives flow across the reef and into a lagoon (Figure 1a). This process is often modeled using the radiation stress approach to wave-mean flow interaction presented by Longuet-Higgins and Stewart (1962). Written for the one-dimensional (1D) reef profile in Figure 1a, the steady, depth-averaged mass and momentum equations, are respectively (Mei 1989)

$$\frac{dq}{dx} = 0 \tag{1}$$

$$\frac{d}{dx}\left(\frac{q^2}{h+\bar{\eta}}\right) = -g\left(h+\bar{\eta}\right)\frac{d\bar{\eta}}{dx} - \frac{1}{\rho}\frac{dS_{xx}}{dx} - \frac{\tau_b}{\rho}, \tag{2}$$

where x is the cross-shore distance, h is the water depth, τ_b is the bed stress, and $q = U\left(\bar{\eta}+h\right)$ is the volume flux per unit width based on the Lagrangian mean velocity $U = U^E + U^S$ (i.e., the sum of an Eulerian velocity U^E and Stokes drift U^S). The radiation stress S_{xx} for normally incident waves is generally computed from linear wave theory as

$$S_{xx} = E_w\left[\frac{2kh}{\sinh\left(2kh\right)} + \frac{1}{2}\right], \tag{3}$$

where k is the wave number and $E_w = 1/8\rho g H_{rms}^2$ is the wave energy density inferred from the root-mean-squared wave height H_{rms}.

A number of attempts have been made to develop simplified analytical solutions to (1)-(3) to predict setup and wave-driven flows on reefs, e.g., Symonds et al. (1995), Hearn (1999 - hereinafter H99), and Gourlay and Colleter (2005 - hereinafter GC05). The simplest of these approaches, e.g.

PRELIMINARY ACCEPTED VERSION

AMERICAN METEOROLOGICAL SOCIETY 1919

H99, consider an incident monochromatic wave of height H_0 and period T, and assume the wave height H through the surfzone is depth-limited by

$$H = \gamma\left(h + \bar{\eta}\right), \tag{4}$$

where γ is an empirical breaking parameter (note that for natural reefs with random wave forcing H_{rms} is typically assumed for H). For the case where γ is spatially uniform, H99 neglects convective accelerations and friction in (2), and using (4) predicts the maximum setup on the reef $\bar{\eta}_r$ will be

$$\bar{\eta}_r = \frac{H_0 - H_r}{\gamma + 8/(3\gamma)}, \tag{5}$$

where $H_r = \gamma h_r$ is the depth-limited wave height over the reef flat. An alternative approach for predicting $\bar{\eta}_r$ was developed by GC05, who empirically related $\bar{\eta}_r$ to the incident wave energy flux (proportional to $H_0^2 T$) and the overall energy dissipated within the surfzone. Consistent with the H99 model result [(5)], the GC05 model also predicts that setup will increase above some breaking wave threshold height H_r, i.e., setup will be absent when $H_0 < H_r$.

The difference in the mean water level between the reef $\bar{\eta}_r$ and the lagoon $\bar{\eta}_L$ can drive an Eulerian flow U_r^E across the reef (Figure 1). For $\bar{\eta}_r << h_r$, and assuming negligible wave dissipation on the reef flat (i.e., $dS_{xx}/dx \approx 0$) where $dh/dx \approx 0$, (2) predicts that a balance will exist between the mean water level gradient and the bed stress. In current-dominated systems (i.e. $U_r^E >> U_w$ where U_w is a representative near-bed wave velocity), bed stresses are often well-described using a quadratic drag law $\tau_b = \rho C_D \left|U^E\right| U^E$ with drag coefficient C_D, such that

$$\frac{d\bar{\eta}}{dx} \approx -\frac{C_D \left|U_r^E\right| U_r^E}{g h_r}; \tag{6}$$

PRELIMINARY ACCEPTED VERSION

in which case $d\bar{\eta}/dx$ can be estimated as $(\bar{\eta}_r - \bar{\eta}_L)/L_r$ given a cross-shore reef flat length L_r (Figure 1a). To obtain a solution to (6), H99 and GC05 assumed in their models that $\bar{\eta}_L$ was approximately zero such that $d\bar{\eta}/dx$ could be estimated as $\sim \bar{\eta}_r / L_r$. This may be a reasonable assumption for those reefs which do not bound land masses or enclosed bodies of water. Examples of such reefs can be found in the 'open' Indo-Pacific atolls that form incomplete rings, or in many of the smaller individual reefs forming the Great Barrier Reef which lack a true lagoon. However, many reefs that form adjacent to coastal land masses, e.g., 'fringing reefs', have enclosed lagoons in which exchange with the surrounding ocean is often restricted by friction through narrow, rough, and sometimes tortuous channels. Assuming $\bar{\eta}_L \sim 0$ for these reef systems may no longer be valid, given that $\bar{\eta}_L$ may become a substantial fraction of $\bar{\eta}_r$ (Jago et al. 2007). Therefore, while $\bar{\eta}_r$ may still be primarily controlled by incident wave forcing under these circumstances, the magnitude of U_r^E should also depend strongly on the momentum dynamics governing $\bar{\eta}_L$.

The overall dynamics controlling wave-driven flows on coastally-bounded reefs may be similar to those, for example, governing rip currents that form over submerged bars on sandy beaches. In this case, setup gradients can drive a flow over a shallow bar crest that returns to the ocean through narrow rip channels (e.g., see MacMahan 2006 for a review). However, while the beach literature may serve as a foundation for understanding and predicting wave-driven flows on coastally-bounded reefs, these reefs may possess a number of key differences that could significantly distinguish their dynamics from beaches. First, the bottoms of coral reefs are often very rough compared to sandy beaches, due to the presence of canopy-forming benthic organisms and the irregular morphology of the platforms on which they grow. The resulting bottom friction generated can play an important or even dominant role in the overall wave-energy dissipation on the forereef (Roberts et al. 1975; Lowe et al. 2005), which could significantly reduce wave setup (Longuet-Higgins 2005; Dean and Bender 2006). Over the reef flat,

PRELIMINARY ACCEPTED VERSION

this enhanced friction may also significantly reduce wave-driven mean flows in comparison to hydraulically smoother beaches. Second, reefs display a much wider range of lagoon and channel geometries than beaches, for example, ranging from the very deep (>50 m) lagoons of atolls to the much shallower (<5 m) lagoons of fringing reefs. Finally, reefs exhibit a wide range of forereef bottom slopes that can vary from order 1:100 to order 1:1. Given that setup on reefs and beaches is strongly slope dependent (Stockdon et al. 2006, Callaghan et al. 2006), the relationship between incident wave forcing and wave setup on reefs may differ appreciably from beaches.

The main objective of this paper is to investigate how the fundamental momentum balances governing wave setup and circulation on coastal reefs behave under different incident wave conditions, and how these balances are affected by reef morphology. To accomplish this, a detailed investigation into the dynamics of wave-driven flows in Kaneohe Bay, Hawaii was conducted (Figure 2) using observations from a 10-month field program. The influence of winds, tides and buoyancy on the lagoon circulation of Kaneohe will be presented elsewhere. Previously, the most detailed physical oceanographic study of this system was conducted by Bathen (1968), who did not consider wave forcing. In contrast, H99 proposed that Kaneohe Bay's reef and lagoon are dominantly flushed by wave-driven flows; this conclusion was based largely on the model discussed above, due to the lack of any detailed field observations. To aid in the interpretation of the wave setup and circulation observations, as well as to broaden the scope of the study, a simple model that considers the mass and momentum balances governing setup and circulation in the cross-reef direction (both over the reef flat and within the lagoon-channel region) is developed. Through application of this model, we are able to investigate how key properties (e.g., frictional characteristics and reef morphological parameters) associated with coastal reefs, govern setup and circulation within these systems in a more general way.

This paper is organized as follows. In section 2 we formulate a simple model for estimating setup and circulation on coastally-bounded reefs that extends the 1D mass and momentum balances

PRELIMINARY ACCEPTED VERSION

traditionally considered in the reef literature for the forereef and reef flat regions, to also incorporate the coupled dynamics of the lagoon-channel return flows. A description of the study site, field program and data analysis is presented in section 3. Results from the field studies are described in section 4 and compared with the numerical model predictions and existing reef models in section 5. The results are summarized and discussed in section 6.

2 Wave-driven reef circulation in the presence of lagoon setup

We consider an idealized reef-lagoon-channel cell (Figure 1b) where setup generated by wave breaking drives flow across a shallow reef flat, through a deeper lagoon, and finally exits through a channel. For this reef geometry, mass conservation [(1)] implies that

$$U_r h_r W_r = U_c h_c W_c , \tag{7}$$

where h_r and h_c are representative depths of the reef and channel regions, respectively, W_r and W_c are the alongshore reef and channel widths, and U_r and U_c are the depth-averaged mass transport velocities (i.e., the sum of the Eulerian and Stokes drift velocities). In terms of the total circulation cell width $W_{total} = W_r + W_c$, (7) can be rewritten as

$$\frac{U_c}{U_r} = \frac{\left(W_r / W_{total}\right)}{1-\left(W_r / W_{total}\right)} \frac{h_r}{h_c} . \tag{8}$$

For cases where $\bar{\eta} / h << 1$ (valid for this study site but not always for reefs), the cross-shore momentum balance [(2)] simplifies to

$$\frac{d\bar{\eta}}{dx} = -\frac{1}{\rho g h}\frac{dS_{xx}}{dx} - \frac{\tau_b}{\rho g h} + \frac{q^2}{g h^3}\frac{dh}{dx} . \tag{9}$$

If $\bar{\eta}$ is not small relative to h, the full momentum balance given by (2) must be considered. Although the wave-driven flow pattern in Figure 1b is two-dimensional (2D), i.e., some alongshore flow must be present from the lagoon to the channel, analogous 1D models developed for predicting rip currents on barred-beaches have often found (9) can still provide accurate estimates of cross-shore variations in $\bar{\eta}$

PRELIMINARY ACCEPTED VERSION

(e.g., Dalrymple et al. 1978; Reniers and Battjes 1997; Bellotti 2004). This is because the along-beach variability in $\bar{\eta}$ driving these flows is often controlled by alongshore variability in the dominant cross-shore momentum balances, e.g., as computed between separate cross-shore transects over both the bar and through a rip channel. Nevertheless, it is always important to evaluate the performance and inherent assumptions of these simple models, as is done below using the field dataset.

Given a prediction of $S_{xx}(x)$, (9) can be numerically integrated across the reef (along transect *A*-*B*, see Figure 1b) for a given cross-reef discharge q_r, from offshore ($\bar{\eta} = 0$) to the lagoon ($\bar{\eta} = \bar{\eta}_L$):

$$\bar{\eta}_L = \int_{x=-\infty}^{x=L_r} \left(-\frac{1}{\rho g h}\frac{dS_{xx}}{dx} - \frac{C_{D,r}\left|q_r^E\right|q_r^E}{gh^3} + \frac{q_r^2}{gh^3}\frac{dh}{dx} \right) dx, \qquad (10)$$

where $C_{D,r}$ is a representative drag coefficient for the reef flat. Note that in wave-dominated coastal regions (i.e., $U_w >> U_r^E$), a linear drag law may be more appropriate yet can easily be substituted into (10), i.e., $\tau_b = \rho C_D' U_w U_E$, with a linear drag coefficient C_D' (Mei 1989).

Equation (1) requires q_r to be constant along *A*-*B*, however, otherwise remains unconstrained by the offshore boundary condition ($\bar{\eta} = 0$), i.e. a valid solution for $\bar{\eta}_L$ in (10) can be obtained for any q_r. Thus to evaluate q_r, the additional momentum balance on the lagoon-channel return flow is also considered. If it is assumed that 1) wave-forcing is negligible in this deep channel region (i.e., $dS_{xx}/dx \approx 0$), 2) h_c is spatially uniform in this region (i.e., $dh/dx \approx 0$), and 3) Stokes drift is negligible (i.e., $q_c^E \approx q_c$), then the simplified momentum balance [(2)] becomes

$$\frac{d\bar{\eta}}{dx} \approx -\frac{C_{D,c}\left|q_c\right|q_c}{gh_c^3} \qquad (11)$$

where $C_{D,c}$ is a representative drag coefficient for this lagoon-channel region (possibly different from the reef value $C_{D,r}$). Given that $\bar{\eta}$ should eventually return to zero out the channel, the lagoon-

PRELIMINARY ACCEPTED VERSION

channel water level gradient in (11) can be estimated as $d\bar{\eta}/dx \approx \bar{\eta}_L / L_c$, where L_c can be taken as the total return flow path (transect *B-C-D,* see Figure 1b). This gives

$$\bar{\eta}_L = \frac{C_{D,c} q_c^2 L_c}{g h_c^3} = \frac{C_{D,c} L_c}{g h_c^3} \left(\frac{W_r}{W_c} \right)^2 q_r^2 , \qquad (12)$$

where flow through the channel q_c has been related to the flow across the reef q_r using (7). (10) and (12) represent a closed set of equations that can be numerically solved by first guessing a value of q_r, evaluating $\bar{\eta}_L$ using (10), comparing this value with $\bar{\eta}_L$ predicted from (12), and then iterating to find a q_r that satisfies both (10) and (12).

A wave model is needed to predict cross-shore variation in S_{xx} for (10). A number of 1D models have been developed to predict wave transformation on beaches (e.g., Thornton and Guza 1983; Lippmann et al. 1996; Baldock et al. 1998); these models should also be appropriate for reefs with relatively mild slopes (e.g., <1:10). It is not the goal of the present study to conduct a detailed evaluation of such wave models (for such a review see Apotsos et al. 2008a). For this application, the model by Thornton and Guza (1983) (hereinafter TG83) is applied, in part because it was found to accurately predict wave transformation on the Kaneohe reef in prior work (Lowe et al. 2005). Like many parametric wave models, TG83 assume that cross-shore gradients in wave energy flux are balanced by the local rate of energy dissipation by both breaking ε_b and bottom friction ε_f,

$$\frac{d}{dx}\left(E_w c_g \right) = -\varepsilon_b - \varepsilon_f , \qquad (13)$$

where ε_b and ε_f are parameterized via semi-empirical relationships. Given E_w, S_{xx} is evaluated with (3). While the enhancement of S_{xx} by rollers is sometimes added to (3), this is not included in the present study. We note, however, that some studies of beaches have found that the inclusion of a roller

PRELIMINARY ACCEPTED VERSION

has only a minimal effect on the total setup generated shoreward of the surfzone (e.g., Apotsos et al. 2007).

3 Field experiment

3.1 Site description

Kaneohe Bay (Figure 2), located on the northeast coast of Oahu, Hawaii (21°29′ N, 157°48′ W) is approximately 13 km long by 4 km wide. A 5 km long, ~2 km wide, shallow (<3 m) reef extends over much of the area, and is covered by coral, algae, coral rubble and sand. An ~1 km wide lagoon (12-16 m deep) separates the reef from shore, with a bottom comprised mostly of sand and mud, although there are a number of coral patch reefs that rise to within ~1 m of the surface distributed throughout. The lagoon exchanges with the ocean through the northern Ship Channel (mean depth ~12 m) and the shallower Sampan Channel in the south (mean depth ~5 m).

3.2 Measurement of waves, currents and wave setup

A series of instrument deployments were conducted between June 2005 and March 2006 (Table 1). Waves were measured by an offshore directional wave buoy (WO), two Seabird Electronics (SBE) pressure sensors (model 26) located on the forereef (W1, W2), two on the back reef (W3, W4), as well as the pressure sensors on three RD Instruments Acoustic Doppler Current Profilers (ADCPs) located on the reef flat (A2, A3, A4) (Table 1). The offshore wave buoy, operated and maintained by the University of Hawaii Sea Level Center, was located ~8 km south-east of Mokapu Point. SBE 26s at sites W1 and W2 each collected 2048 pressure samples at 2 Hz every 30 minutes, while at W3 and W4 collected 1024 samples at 1 Hz every hour. The ADCPs at sites A2, A3, and A4 were burst sampled such that 900 pressure samples were obtained at 1 Hz every hour. An additional SBE 26 was operated as a water level gauge (no waves) and was positioned on a patch reef in the lagoon (site W5).

Pressure data were analyzed by dividing each burst into 16 sections of equal length, each with 50% overlap, applying a Hanning window to the segments, and computing spectra. These were converted to one-dimensional wave spectra S using linear wave theory, from which rms wave heights

PRELIMINARY ACCEPTED VERSION

were calculated as $H_{rms} = (8m_0)^{1/2}$, where m_0 is the zeroth moment of S based on the energy between 2 and 30 s (this generally contained >99% of the total wave energy). Mean T_{m01} and peak T_p wave periods were subsequently calculated based on the first spectral moment of S and the spectral peak, respectively. At deeper sites (W1 and W2), the spectra between 2 and 4 s was modeled by assuming a frequency to the -4 power relationship (Jones and Monismith 2007), in order to account for energy that could not be resolved in this high frequency region due to the attenuation of the pressure signal with depth. This correction generally only contributed a small amount (<2%) to the total energy.

Theories developed to predict $\bar{\eta}_r$ on reefs are often cast as dependent on the deep-water wave height $H_{rms,0}$. However, because of large-scale wave refraction, wave heights measured by the offshore wave buoy (site WO) may not accurately reflect the deep water wave height directly offshore of the study site. $H_{rms,0}$ was therefore calculated from the rms wave height measured on the forereef H_{FR}, corrected to a deep water value using a shoaling coefficient $K_s = H_{FR} / H_{rms,0}$ (Dean and Dalrymple 1991) based on the peak period T_p. K_s was generally close to unity throughout the experiment (range 0.90-1.05; mean 0.94).

Current profiles were measured using seven ADCPs deployed at sites A1-A7, with bin sizes ranging from 0.05 to 0.5 m (Table 1). All of the ADCPs were burst sampled at 1 Hz for 15 minutes each hour. Hourly current profiles were obtained for each ADCP by averaging all samples in a burst and were depth-averaged to produce time-series of U^E. These were rotated into the principal component axes of the velocity variance (Emery and Thompson 2001), such that positive flow along the major axis represented flow into the bay. Tidal current amplitudes and phases were calculated from U^E using T_TIDE (Pawlowicz et al. 2002). A correlation coefficient R_{tide} for currents is thus defined as the square-root of the percentage of total variance in U^E explained by the tidal harmonic analysis.

PRELIMINARY ACCEPTED VERSION

No sites were located inside the surfzone, so the wave-induced transport was estimated from the depth-averaged Stokes drift velocities U^S computed from the wave spectra following Kenyon (1969). Given that most wave measurements did not include directional information, the dominant Stokes drift directions were inferred from directions output from a numerical wave model (SWAN – Booij et al. 1999) simulation of the winter experiment. Wave directions in Kaneohe Bay were mostly insensitive to large variations in offshore wave direction, since they are mainly controlled by refraction patterns over the shallow reef (Lowe et al. 2005).

Mean water level variability $\bar{\eta}$ (defined relative to still water) at this site was driven by tides and wave setup, since wind-setup was estimated to be only O(1 mm) based on a typical 5 m s^{-1} wind speed (Lugo-Fernandez et al. 1998) and thus could be neglected from the momentum balance. Although wave setup on both reefs and beaches can be modulated at tidal frequencies (e.g., Thornton and Kim 1993; MacMahan et al. 2006), discriminating these relatively small modulations in setup from much larger variations in the tides occurring at the same frequencies can be difficult. Through application of the model from section 2, we estimated these tidal modulations in setup to be relatively insignificant in comparison to the much greater variability in $\bar{\eta}$ resulting from observed changes in incident wave forcing (not shown). Therefore, in the present study, the specific response of both setup and currents to incident wave forcing was investigating at sub-tidal frequencies by applying a PL64 filter (Beardsley et al. 1985) with a half-power period of 38 hours. Although performing a similar analysis at higher frequencies poses an interesting problem, it is beyond the scope of the present paper and, moreover, not necessary for exploring the fundamental dynamics given in (2). For consistency, when investigating relationships between setup, currents, and wave forcing, each pair of time series were low-pass filtered identically and then decimated to six hourly values to form a "subtidal" data set. In all calculations, significance levels were obtained from the effective degrees of freedom (DOF)

PRELIMINARY ACCEPTED VERSION

AMERICAN METEOROLOGICAL SOCIETY 1919

estimated from the record length divided by the autocorrelation timescale (Davis 1976); this timescale was typically ~1.5-2 days.

To compute wave setup, a modified version of the approach by Raubenheimer et al. (2001) was used, which is detailed in Appendix A. Setup was calculated only for sites where instruments were deployed on a hard reef platform (i.e., A2-A4, W3-W5). Thus, data collected by instruments in the channels (A1 and A5) were precluded from the analysis, since they gradually sank into the sand by up to 5 cm during the experiment, making it difficult to maintain an accurate reference level. Note that data from sites A2 and A3 was used to estimate the maximum reef setup $\bar{\eta}_r$, since they were located only ~100-200 m shoreward of a consistent surfzone (Figure 1). This is equivalent to only 5-10% of the overall-cross reef length L_r, so given the momentum balance in (6), $\bar{\eta}$ measured at these sites should be at most 5-10% less than $\bar{\eta}_r$.

4 Observations

4.1 Offshore forcing conditions

The winter deployment captured four spring-neap tidal cycles (Figure 3a) and offshore rms wave heights $H_{rms,0}$ averaged 1.6 m (Figure 3b). During the first two weeks (18-30 January), trade-wind wave conditions dominated, with persistent waves coming from the east with $H_{rms,0} \sim 2$ m and $T_p \sim 7-9$ s. For the remainder of the experiment, waves were variable ($H_{rms,0} \sim$ 1-3 m; $T_p \sim 6-13$ s), in part generated remotely by several North Pacific storms. $H_{rms,0}$ over the longer 10-month deployment (not shown) averaged ~1.4 m (range ~0.5-3.5 m), and propagated mostly from $50^o - 80^o$.

4.2 Wave energy distribution

Figure 4a shows time-series of measured H_{rms} at representative forereef and reef flat sites. H_{rms} on the forereef (sites W1 and W2) was on average 25% lower than offshore (Table 2), with only ~6% of this discrepancy explained by wave shoaling (see section 3.2). As discussed by Lowe et al. (2005), this

PRELIMINARY ACCEPTED VERSION

wave attenuation is likely caused by bottom friction across the rough and relatively gently-sloping forereef offshore of sites W1 and W2.

In general, wave heights in Kaneohe Bay can be controlled by changes to either offshore wave conditions or tidal elevation (or a combination of both). To quantify these effects, correlation coefficients between the local wave height and both the offshore wave height and local water depth were computed (Table 2). Wave heights on the forereef (W1 and W2), measured prior to breaking, were only correlated with offshore wave heights (R_{wave}~0.9), while on the shallow reef flat (A2 and A3) were instead primarily controlled by the tidal elevation (R_{tide}~0.8). Thus, given that A2 and A3 sit shoreward of a saturated surfzone, local wave heights were mostly insensitive to changes in incident wave forcing (Figure 4a) since their height was depth-limited according to $H_{rms,\max} = \gamma_r h_r$. The measurements indicate $\gamma_r \approx 0.3$ at sites A2 and A3 (Figure 4c), comparable to values found on other reefs and also on some beaches (e.g., Thornton and Guza 1982; Hardy and Young 1996). At A4, W3 and W4, all located on the reef but in deeper water (~3-5 m), wave heights were only weakly correlated with tides (R_{tide}<0.5) and were more correlated with the offshore wave height (R_{wave}~0.6-0.8).

4.3 Dominant circulation patterns

On-average, two persistent circulation cells dominated the north and south regions of the bay (Figure 5a), with onshore flow generated over the shallow reef sections (A2 and A3) followed by return flows out the channels (A1 and A5); the division of these cells occurred at Kapapa Island, roughly at the alongshore center of the bay. The major axes of the principal component ellipses at most sites were aligned with time-averaged current vectors (Figure 5b). Mean flow inside the lagoon (A6 and A7) was typically much weaker than over the reef, averaging ~1-2 cm s^{-1}, however, instantaneously attained values up to ~10 cm s^{-1} (Figure 6c).

Variability in U_E occurring at tidal frequencies may result from a combination of the ebbing and flooding of the bay, as well as tidal modulations of the wave-driven currents. On the reef (A2-

PRELIMINARY ACCEPTED VERSION

A4), these tidal flows were oriented across the reef; note that at A4 this implies that the flow was roughly orthogonal to the dominant flow direction at this site (Figure 5d). Tidal currents were much stronger in the channels and lagoon than over the reef (by factors ranging from 2-4), due to preferential flow through these deeper regions (Table 3). In general, flow variability inside the lagoon (A6 and A7) was dominantly driven by tides, with R_{tide} ranging between 0.7-0.8. Flow variability in the channels (A1 and A5) was only partially correlated with tides (R_{tide} = 0.5-0.6), with very weak correlation R_{tide} <0.3 on the reef flat (A2 and A3).

4.4 Wave-driven transport

To evaluate the role of wave-forcing, the response of the subtidal circulation to the magnitude of $H_{rms,0}$ was investigated. Subtidal flows across the reef (A2, A3 and A4) and in the channels (A1 and A5) were dominantly wave-driven (Figure 6a,b), with R_{wave} ~ 0.8-0.9. However, for the lagoon sites (A6 and A7), subtidal currents were only weakly correlated with $H_{rms,0}$ (R_{wave} <0.3) (Figure 6c).

For the reef and channel sites where subtidal flows were dominantly wave-driven (Figure 6a,b), U^E increased roughly linearly with $H_{rms,0}$. Moreover, a threshold wave height H_r was apparent at these sites, corresponding to the point where the wave-driven circulation roughly shut down (see Figure 6a,b). H_r was evaluated for each site (based on the rms wave height) and averaged $H_r = 0.7$ m (range 0.6-0.8 m) (Table 3). Given the typical Kaneohe reef flat depth $h_r \approx 2$ m (Falter et al. 2004), the ratio observed $H_r / h_r \approx 0.35$ is similar to the $H_r / h_r \approx 0.4$ proposed by Gourlay (1996).

Mean Stokes drift vectors during the winter experiment were directed across the reef (Figure 5c). Computed U^S was most variable on the forereef (range ~1-16 cm s^{-1}; mean ~3 cm s^{-1}) but on average was comparable to values on the reef at A2 and A3 (range ~1-5 cm s^{-1}; mean ~3 cm s^{-1}). On the reef, Stokes drift on-average contributed ~25% of the total transport but its importance varied as offshore wave conditions changed (Figure 7). Given that waves on the reef (sites A2 and A3) were

PRELIMINARY ACCEPTED VERSION

AMERICAN METEOROLOGICAL SOCIETY 1919

mostly independent of offshore wave conditions, the relative importance of Stokes drift increased as the incident wave forcing decreased to a point where it sometimes dominated over the Eulerian flow.

4.5 Wave setup

A strong correlation was present between $\bar{\eta}$ and $H_{rms,0}^2 T_p$ for representative sites on the reef flat and lagoon (Figure 8b,c), indicating that setup increased roughly proportionally to the incident (deep water) wave energy flux. Results of a nonlinear least squares fitting of $\bar{\eta} = aH_{rms,0}^m T_p^n - b$ [(15)] to the data indicated that *m* and *n* ranged between 1.8-2.9 and 0.7-1.0, respectively, averaging $m = 2.3$ and $n = 0.8$ (Table 4). This scaling is very different from the $m = 1$, $n = 0$ scaling from H99 [(5)], but consistent with the $m = 2$, $n = 1$ scaling of GC05.

Spatial variations in $\bar{\eta}$ are illustrated in Table 4, where values were calculated for $H_{rms,0} = 2$ m and $T_p = 7$ s using the nonlinear regression coefficients computed for each dataset. For this wave condition, $\bar{\eta}_r \sim 6-8$ cm on the reef flat (A2 and A3) and ~4 cm on both the back reef (W3 and W4) and lagoon (W5). Thus, $\bar{\eta}_L$ was not zero inside the lagoon (Figure 8a) as assumed in existing reef models, instead representing ~60-80% of the maximum reef flat values $\bar{\eta}_r$. Wave setup also varied somewhat alongshore (Table 4). For a given wave height, $\bar{\eta}$ was largest at the shallowest reef flat sites (A2 and A3) near the alongshore center of the bay and slightly smaller at the deeper site (A4). This is not surprising since over this shallower section of reef, more wave energy was dissipated by breaking, and also when comparing equal rates of dissipation, setup gradients will increase in shallower water via (2).

5 Model application

To apply the model in section 2 to Kaneohe, we first defined representative reef geometry parameters (i.e., L_r, W_r, h_r W_c, h_c and forereef slope). Given that the water depth is not uniform over the reef and channel regions, we assigned uncertainties to these depths based on the typical range within each region, and propagated this uncertainty through the calculations via Monte Carlo simulations.

PRELIMINARY ACCEPTED VERSION

Therefore, a representative reef flat depth would be $h_r = 2 \pm 1$ m, while the depths of the southern and northern channels were assigned $h_c = 5 \pm 2$ m and 12 ± 3 m, respectively. A forereef slope (~1:60) was taken from Lowe et al. (2005) (see Figure 15 in that paper). The overall widths of the two circulation cells W_{total} were defined as the distances from Kapapa Island to the northern and southern extent of the channels (Table 5). Apportioning W_{total} between channels and reef can be done by calculating the slope from a linear regression of U_c versus U_r for each cell (Figure 9), to estimate the fraction of the total cell W_r / W_{total} required to account for the observed flow exiting the channels via (8). This gave $W_r / W_{total} = 0.71 \pm 0.16$ and 0.73 ± 0.13 for the southern and northern cells, respectively (Table 5).

Both (10) and (12) assume a quadratic drag law holds; however, for cases where $U_w >> U^E$, a linear drag model may be more suitable (e.g., Mei 1989). Choosing an appropriate drag law is important, since this will directly control how the reef circulation scales with incident wave forcing, i.e.: U_r^E will scale according to $H_{rms,0}$ (or $\bar{\eta}_r^{1/2}$) if drag is quadratic, and to $H_{rms,0}^2$ (or $\bar{\eta}_r$) if drag is linear. On the reef flat (A2-A3) where wave heights were mostly time-invariant (Figure 4a), a typical rms near-bed wave velocity was $U_w \sim 0.4\,\mathrm{m\,s^{-1}}$, making U_w comparable to U_r^E and thus ambiguous as to which drag form should be applied. Therefore, a quadratic drag law was considered; however, for the sake of completeness the influence of a linear formulation on the model results was investigated. A linear regression between the setup and current data was then used to compute quadratic drag coefficients assuming an estimated cross-reef length $L_r = 1500 \pm 200$ m and lagoon-channel return path $L_c = 5000 \pm 2000\,\mathrm{m}$ for both cells (Figure 10). Reef $C_{D,r}$ and lagoon-channel $C_{D,c}$ drag coefficients (estimated from (6) and (11), respectively) were generally comparable and also similar for both the southern and northern cells, ranging between 0.01 and 0.03 (Table 5). A similar analysis was also conducted to calculate linear drag coefficients (not shown); however, this required estimating U_w

PRELIMINARY ACCEPTED VERSION

which spatially decayed across the reef flat. Given that U_w typically ranged from 0.4 m s^{-1} on the leading edge of the reef flat (A2-A3) to zero on the back reef, for simplicity a spatially-averaged 0.2 m s^{-1} was assumed for the system. This gave values of $C'_{D,r}$ and $C'_{D,c}$ for the reef and lagoon-channel regions, respectively, ranging between 0.01 and 0.02 (Table 5), thus similar to the quadratic coefficients.

To illustrate the predicted cross-shore variation in H_{rms}, $\bar{\eta}$, and U^E over the reef for the southern cell, we first considered a 'typical' wave condition as an example ($H_{rms,0} = 2$ m, $T_p = 7$). The TG83 wave model was applied both with friction present [i.e., using the energy dissipation factor $f_e = 0.24$ measured on the Kaneohe reef by Lowe et al. (2005)] and with friction turned off. We assumed a spatially-uniform $C_D \sim 0.02$, given the similarity between measured $C_{D,r}$ and $C_{D,c}$ (see above). In addition, we assumed an initial offshore wave height that reproduced the same H_{rms} on the forereef (i.e., as directly measured at site W1) *after* the effects of shoaling and friction had been assessed. Thus, including friction required a slightly larger initial $H_{rms,0} = 2.4$ m to produce the same forereef H_{rms} (Figure 11b), implying that frictional damping offshore of W1 reduced the wave height by ~20%, which is comparable to the difference observed between the forereef and offshore wave buoy (Table 2). When compared to the no-friction case, the inclusion of friction also significantly reduced H_{rms} on the reef flat, which gradually decayed shoreward.

Although the model slightly overpredicted observed $\bar{\eta}_r$ and $\bar{\eta}_L$ by ~20%, it did predict that $\bar{\eta}_L$ will be ~60% of $\bar{\eta}_r$, a ratio consistent with observations (Figure 11c). Furthermore the model also matched observed U_r^E when setup in the lagoon was accounted for (Figure 11d). However, because the height of waves incident to the surfzone was fixed for comparison purposes, there were no appreciable differences in both $\bar{\eta}$ and U^E between the runs with and without wave friction. In simulations of the

PRELIMINARY ACCEPTED VERSION

winter experiment period, the model based on the default quadratic drag law reproduced U_r^E well, but tended to slightly underestimate the variability in current fluctuations that result from variation in $H_{rms,0}$ (Figure 12). The model with linear drag tended to better reproduce this wave-driven variability in U_r^E, but overpredicted the amplitude of the current fluctuations some of the time. Finally, the model also indicated that Stokes drift should be the dominant transport mechanism on the forereef and also in the vicinity of the reef crest (Figure 11e).

In contrast, it is clear that H99 [via (5)] significantly overpredicts $\bar{\eta}_r$ (by a factor ~3) (Figure 11c). While the H_{rms} distribution from H99 [via (4)] correctly predicted the total reduction in H_r by breaking (not surprising since the observed $\gamma_r = 0.3$ was used), the decrease in H_{rms} through the surfzone occurs much more rapidly than predicted by TG83 (Figure 11b), which led to much stronger radiation stress gradients that enhanced $\bar{\eta}_r$. Combined with the fact that H99 neglects lagoon setup, it overpredicted U_r^E by a factor of ~2. GC05 do not attempt to predict the particular H_{rms} distribution and instead relate $\bar{\eta}_r$ to the total dissipation in the surfzone, which increases proportionally to an empirical "reef profile shape factor" K_p that they find increases with reef slope from ~0.2 to 0.8 [see (17) in their paper for details]. While GC05 with $K_p = 0.8$ overpredicted $\bar{\eta}_r$ by a factor of ~4 (not shown), predictions using $K_p = 0.2$ were in good agreement with observations (Figure 11c). Nonetheless, GC05 still overpredicted U_r^E by ~20%, due to the model's neglect of $\bar{\eta}_L$.

6 Discussion and conclusions

6.1 Wave-driven circulation of Kaneohe Bay

Results from the study revealed that wave breaking was the dominant mechanism driving flow over the reef flat and out the reef channels. Comparison of the reef flat (A2 and A3) and channel (A1 and A5) current speeds, showed that the effective reef width W_r of each circulation cell was ~3 times larger

PRELIMINARY ACCEPTED VERSION

AMERICAN METEOROLOGICAL SOCIETY 1919

than the corresponding channel width W_c, indicating that the bulk of the total alongshore reef length supported an onshore wave-driven flow.

In contrast, the weaker subtidal currents in the lagoon (A6 and A7) suggested that wave forcing may play a much smaller role in the overall lagoon circulation. To some degree this is expected, since the cross-sectional area of the deep lagoon ($h_L L_L \sim 16{,}000$ m^2) is much greater than the cross-sectional area of each reef cell ($h_r W_r \sim 4000$ m^2). Consequently, an average reef current speed $U_r \sim 0.1$ m s^{-1} (Table 3) would only induce a lagoon current $U_L \sim 0.02$ m s^{-1}, if it is assumed that mass is conserved across the reef to lagoon (i.e., $U_r h_r W_r = U_L h_L L_L$). As a result, any wave-driven current signal measured in the lagoon should indeed be very weak, and may be comparable or dominated by subtidal currents induced by winds and buoyancy (Bathen 1968). The conceptual model did assume that flow originating near the reef crest (A2 and A3) crosses the entire reef flat before entering the channels; however, it is impossible to precisely quantify how much of the total flow crossing the reef directly penetrated into the lagoon from limited point measurements of these very weak lagoon currents. It is possible that only some fraction of the volume of water initially crossing the reef (A2 and A3) actually entered the lagoon, and for example, fed the channels along the back edge of the reef. This would serve to reduce the return flow path length L_c; however, we note that in the calculations we assigned L_c to have a large (40%) uncertainty for this very reason. A reduced L_c would ultimately increase our estimates of $C_{D,c}$ since both q_c and $\overline{\eta}_L$ in (12) are fixed by the measurements (Figure 10). Regardless, any uncertainty in L_c should not alter the dominant momentum balances governing setup and circulation in this system.

Further support for the robustness of using 1D cross-shore mass and momentum equations in this inherently 2D system, is that it appears to provide accurate estimates of both setup and wave-driven transport. However, this is not entirely surprising given that many beach studies have also

PRELIMINARY ACCEPTED VERSION

found that the application of these same 1D equations along a sequence of transects alongshore can often be sufficient for estimating flows that may be ultimately 2D in terms of their spatial structure. For example, for topographic rip currents, Bellotti (2004) used data from Haller et al. (2002) to show that consideration of two 1D cross-shore momentum transects across a bar and through a rip channel could accurately predict the alongshore setup variability responsible for driving these flows when W_c / W_{total} was small, a reasonable assumption for Kaneohe Bay (Table 5). Other, more general studies of topographic-driven alongshore flows, have shown that when the ratio of cross-shore to alongshore length scales of the bottom topography ($\sim L_r / W_{total}$) is small, a cross-shore momentum balance governed by (2) that neglects gradients in the alongshore component of the radiation stresses (S_{xy}) should accurately predict the alongshore setup gradients that dominate the momentum balances of these flows (e.g. Putrevu et al. 1995; Apotsos et al. 2008b). For the circulation cells in Kaneohe Bay, $L_r / W_{total} \sim 0.4 - 0.7$, which is not very small but still less than unity. In general, the detailed spatial structure of wave-driven flows on reefs can certainly be most accurately captured through direct application of sophisticated 2D coupled wave-circulation numerical models. Nevertheless, this simple model based on a pair of 1D cross-shore momentum balances appears to be a particularly useful tool for illustrating how the morphology and bottom roughness of reefs fundamentally controls setup and circulation in coastally-bounded reef systems.

6.2 Role of reef morphology and roughness on setup and circulation of reefs

Maximum setup $\bar{\eta}_r$ on the Kaneohe reef increased proportional to the incident wave energy flux (i.e., $\bar{\eta}_r \propto H_{rms,0}^2 T_p$), consistent with the scaling proposed by GC05 and also predictions from the TG83 model (Figure 12). However, for the range of incident wave heights encountered during the experiment, the magnitude of $\bar{\eta}_r$ itself (<10 cm) was much smaller than previous observations on steeper atolls and barrier reefs (>50 cm, see Gourlay 1996 for a review). This is apparently due to the

PRELIMINARY ACCEPTED VERSION

mild slope of the Kaneohe reef (~1:60), which serves to reduce $\overline{\eta}_r$ in at least two ways: 1) it allows for significant frictional wave dissipation on the forereef prior to breaking and 2) it alters the dynamics of breaking and distributes the overall rate of dissipation over a wider surfzone. The former effect was apparent in Figure 11b, where it was necessary to initialize the wave model with friction using a ~20% larger $H_{rms,0}$ (or ~40% larger offshore wave energy flux) to generate the same $\overline{\eta}_r$ as the case without friction. The latter effect has been studied in detail on reefs by, e.g., Gourlay (1996) and Nielsen et al. (2008), who showed that for a given incident wave condition, $\overline{\eta}_r$ can increase by a factor of ~4 as forereef bottom slopes increase from order ~1:100 to ~1:1. Combined with the fact that the Kaneohe reef is deep ($h_r \sim 2$ m), compared to many other reefs with crests near mean sea level, the Kaneohe reef also has a much larger threshold breaking height H_r, making setup generation extremely inefficient in this system.

Once $\overline{\eta}_r$ is generated, the strength of the wave-driven flow will ultimately be controlled by the morphology and bottom roughness of the reef-lagoon region shoreward of the surfzone. In a classic view of coral reefs, the mean water level in the lagoon is generally assumed to be approximately equal to the open ocean, i.e., it is assumed that the lagoon and channels are sufficiently deep and/or wide such that friction on the return flow is negligible. Conversely, on beaches setup is traditionally assumed to progressively increase past the break point as wave energy is dissipated gradually shoreward (Bowen 1968). Even in topographic rip systems, where a shoreward flow is present over a bar, frictional resistance in the rip current cell is strong enough, in many cases, to maintain a dominant momentum balance across the bar between setup and radiation stress gradients alone (i.e., Reniers and Battjes 1997; Haller et al. 2002). Reef-lagoon systems such as Kaneohe Bay generally sit somewhere between these two extremes, since $\overline{\eta}_L$ is not negligible yet is still much less than $\overline{\eta}_r$. With the flow across the reef U_r^E specifically controlled by $\overline{\eta}_r - \overline{\eta}_L$, the momentum balance on the return flow that controls $\overline{\eta}_L$

PRELIMINARY ACCEPTED VERSION

must be carefully considered, with particular attention being given to the lagoon-channel geometry. For a given reef geometry (fixed W_r, L_r, h_r and forereef slope) and incident wave forcing, $\bar{\eta}_L$ should increase either when: 1) L_c / h_c increases due to an increase in the return flow path length and/or a reduction of the lagoon-channel depth; or 2) W_c / W_{total} decreases due to a relative reduction in channel width. As an example, the former effect can be investigated using the simple model of Kaneohe Bay by holding the reef geometry and channel width constant, and hypothetically varying L_c / h_c, i.e., by increasing the lagoon and channel depths (Figure 13). For this system, the predicted $\bar{\eta}_r / \bar{\eta}_L$ varies from ~1 for $L_c / h_c \sim 0.005$ to ~0 for $L_c / h_c \sim 0.01$. The variation in $\bar{\eta}_L$ between these two limits causes U_r^E to vary by a factor of ~5.

Finally, bottom roughness and its spatial variability is clearly a key factor controlling U_r^E. On the reef flat, estimates of $C_{D,r} \approx 0.02$ were very similar to values measured on other reefs ($C_{D,r} \approx 0.01 - 0.05$; Lugo-Fernandez et al., 1998; Jones et al., 2008; Hench et al., 2008). Although $C_{D,r}$ is greater than the $C_D \sim O(0.001)$ typically observed on relatively smooth sandy beaches (e.g., Feddersen et al. 2003), this value is still much smaller than the $C_{D,r} = 0.1$ assumed by H99 for Kaneohe Bay. Evidently H99 required such an abnormally high $C_{D,r}$ to produce reasonable currents at this site, given the model's over prediction of $\bar{\eta}_r$ and its neglect of setup inside the lagoon. Estimated lagoon-channel drag coefficients $C_{D,c} \approx 0.01 - 0.02$ were comparable to $C_{D,r}$, suggesting that C_D may be surprisingly uniform across this system. This may be due to the fact that the lagoon and channels are interspersed by numerous 'patch reefs' (biogenic carbonate structures formed by coral that extend over most of the water column; see Figure 1). These patch reefs may locally serve to increase effective C_D's to order 1 or larger (Reidenbach et al. 2006; Monismith 2007) thus augmenting the spatially-

PRELIMINARY ACCEPTED VERSION

integrated $C_{D,c}$'s that were measured. Lastly, both the measurements and model predictions indicate that wave-current interactions on coral reef flats can potentially have a major influence on the response of the system-wide circulation to incident wave forcing, by controlling the scaling of bed stresses with U_r^E. For systems such as Kaneohe, the importance of these wave-current interactions may vary considerably across the system, due to the high degree of spatial variability in wave energy, current speeds, and physical bed roughness.

PRELIMINARY ACCEPTED VERSION

AMERICAN METEOROLOGICAL SOCIETY 1919

Acknowledgements

The authors are grateful to Dan Schar, Pete Newkirk, Nicole Jones, Cameron McDonald, Sarah Giddings and Kristen Davis for assisting with the field experiments, and the constructive comments from two anonymous reviewers and Jerry Smith that helped to greatly improve the original manuscript. SGM thanks Jim Hench for discussions into reef dynamics. We especially thank Jerome Aucan, Mark Merrifield and the Coastal Data Information Program for providing the offshore wave buoy data. This work was supported by the National Science Foundation through grants OCE-0452800, OCE-0453117, OCE-0622967 and OISE- 0601787, and the Singapore Stanford Partnership. RJL acknowledges support from an Australian Research Council Discovery Project grant DP0770094.

PRELIMINARY ACCEPTED VERSION

AMERICAN METEOROLOGICAL SOCIETY 1919

Appendix A: Wave setup analysis

Subtidal mean water level variability $\bar{\eta}$ was evaluated by decomposing the burst-averaged pressure data as $P=P_{atm}+\eta+h$, where P_{atm} is atmospheric pressure, h is the still-water depth, and η is the water level associated with tides and wave setup. We assume that η on the forereef sites (W1 and W2) only varied with tides, i.e. set-down was negligible here (this was justified a posteriori; see Figure 11c). This defines a reference pressure P_0, such that for each site, we obtain $\Delta P = \eta + h - h_0$, where $\Delta P \equiv P - P_0$. We note that possible flow noise effects on ΔP, due to the dynamic pressure field of the waves (see Raubenheimer et al. 2001), were estimated to be negligible based on observed and modeled (via section 5) near-bed wave velocities evaluated between each pair of sites.

Subtidal variability was obtained by applying a PL64 filter (Beardsley et al. 1985) such that

$$\overline{\Delta P} = \bar{\eta} + h - h_0, \qquad (14)$$

where the overbars denote low-pass filtered variables. To evaluate how $\bar{\eta}$ scales with incident wave conditions, note that existing analytical models of reef wave setup $\bar{\eta}$ (see section 1) scale by

$$\bar{\eta} = aH_{0,rms}^{m}T_p^{n} - b, \qquad (15)$$

where a and b are empirical constants and m and n are coefficients describing the scaling of $\bar{\eta}$ with respect to the offshore wave forcing. (14) can then be rewritten as $\overline{\Delta P} = aH_{rms,0}^{m}T_p^{n} - c$, where $c \equiv b - h + h_0$ is a constant for each site. Through a nonlinear least-squares regression of $\overline{\Delta P}$ versus $H_{rms,0}$ and T_p, the coefficients (a, c, m and n) and their uncertainty were evaluated. However, to evaluate the magnitude of $\bar{\eta}$ via (15), the coefficient b must first be calculated given that the pressure sensors were not leveled. This coefficient can be obtained from the current measurements by evaluating the threshold wave height H_r below which the wave-driven circulation turns off (see Figure 6). At this threshold where $H_0 = H_r$, setup $\bar{\eta}$ on the reef is zero such that $b = aH_r^{m}T_p^{n}$.

PRELIMINARY ACCEPTED VERSION

AMERICAN METEOROLOGICAL SOCIETY 1919

References

Apotsos, A., B. Raubenheimer, S. Elgar, R. T. Guza, and J. A. Smith, 2007: Effects of wave rollers and bottom stress on wave setup. *Journal of Geophysical Research-Oceans*, **112**, C02003.

Apotsos, A., B. Raubenheimer, S. Elgar, and R. T. Guza, 2008a: Testing and calibrating parametric wave transformation models on natural beaches, *Coastal Engineering*, **55**, 224-235.

Apotsos, A., B. Raubenheimer, S. Elgar, and R. T. Guza, 2008b: Wave-driven setup and alongshore flows observed onshore of a submarine canyon, *Journal of Geophysical Research*, in press.

Baldock, T. E., P. Holmes, S. Bunker, and P. Van Weert, 1998: Cross-shore hydrodynamics within an unsaturated surf zone, *Coastal Engineering*, **34**, 173-196.

Bathen, K. H., 1968: *A descriptive study of the physical oceanography of Kaneohe Bay, Oahu, Hawaii.,* p. 353. Hawaii Institute of Marine Biology. Technical Report Number 14.

Beardsley, R. C., R. Limeburner, and L. K. Rosenfeld, 1985: *Introduction to the CODE-2 moored array and large-scale data report*, CODE Tech. Rep. 38 and WHOI Tech. Rep. 85-35.

Bellotti, G., 2004: A simplified model of rip currents systems around discontinuous submerged barriers, *Coastal Engineering*, **51**, 323-335.

Booij, N., R. C. Ris, and L. H. Holthuijsen, 1999: A third-generation wave model for coastal regions - 1. Model description and validation, *Journal of Geophysical Research-Oceans*, **104**(C4), 7649-7666.

Callaghan, D. P., P. Nielsen, N. Cartwright, M. R. Gourlay, and T. E. Baldock, 2006: Atoll lagoon flushing forced by waves, *Coastal Engineering*, **53**, 691-704.

Davis, R.E., 1976: Predictability of sea surface temperature and sea level pressure anomalies over the North Pacific Ocean, *Journal of Physical Oceanography*, **6**, 249–266.

Dalrymple, R.A., 1978: Rip Currents and their Causes. *Proc. 16th Intl. Conf. Coastal Engineering, ASCE*, 1414-1427.

PRELIMINARY ACCEPTED VERSION

AMERICAN METEOROLOGICAL SOCIETY 1919

Dean, R. G., and C. J. Bender, 2006: Static wave setup with emphasis on damping effects by vegetation and bottom friction, *Coastal Engineering*, **53,** 149-156.

Dean, R. G., and R. A. Dalrymple, 1991: *Water wave mechanics for engineers and scientists*. World Scientific.

Emery, W. J., and R. E. Thompson, 2001: *Data analysis methods in physical oceanography*. Elsevier.

Falter, J. L., M. J. Atkinson, and M. A. Merrifield, 2004: Mass transfer limitation of nutrient uptake by a wave-dominated reef flat community, *Limnology and Oceanography*, **49**, 1820-1831.

Feddersen, F., E. L. Gallagher, R. T. Guza, and S. Elgar, 2003: The drag coefficient, bottom roughness, and wave-breaking in the nearshore, *Coastal Engineering*, **48**, 189-195.

Gourlay, M. R., 1996: Wave set-up on coral reefs .2. Set-up on reefs with various profiles, *Coastal Engineering*, **28**, 17-55.

Gourlay, M. R., and G. Colleter, 2005: Wave-generated flow on coral reefs - an analysis for two dimensional horizontal reef-tops with steep faces, *Coastal engineering*, **52**, 353-387.

Haller, M. C., R. A. Dalrymple, and I. A. Svendesen, 2002: Experimental study of nearshore dynamics on a barred beach with rip channels, *Journal of Geophysical Research-Oceans* **107**, C6,3061, 10.1029/2001JC000955.

Hardy, T. A., and I. R. Young, 1996: Field study of wave attenuation on an offshore coral reef. *Journal of Geophysical Research-Oceans*, **101**(C6), 14311-14326.

Hearn, C. J., 1999: Wave-breaking hydrodynamics within coral reef systems and the effect of changing relative sea level, *Journal of Geophysical Research-Oceans*, **104**(C12)**,** 30007-30019.

Hench, J.L., J.J. Leichter and S.G. Monismith, 2008: Episodic circulation and exchange in a wave-driven coral reef and lagoon system, *Limnology and Oceanography*, submitted.

PRELIMINARY ACCEPTED VERSION

AMERICAN METEOROLOGICAL SOCIETY 1919

Jago, O. K., P. S. Kench, and R. W. Brander, 2007: Field observations of wave-driven water-level gradients across a coral reef flat, *Journal of Geophysical Research-Oceans*, **112**, C06027.

Jones, N. L., and S. G. Monismith, 2007: Measuring short-period wind waves in a tidally forced environment with a subsurface pressure gauge, *Limnology and oceanography: Methods*, **5**, 317-327.

Jones, N.L., Lowe, R.J., Pawlak, G., Fong, D.A., and S.G. Monismith, 2008: Plume dispersion on a fringing coral reef system, *Limnology and Oceanography*, in press.

Kenyon, K. E., 1969: Stokes Drift for Random Gravity Waves, *Journal of Geophysical Research,* **74**, 6991-6994.

Kraines, S. B., T. Yanagi, M. Isobe, and H. Komiyama, 1998: Wind-wave driven circulation on the coral reef at Bora Bay, Miyako Island, *Coral reefs*, **17**, 133-143.

Lippmann, T. C., A. H. Brookins, and E. B. Thornton, 1996: Wave energy transformation on natural profiles, *Coastal Engineering*, **27**, 1-20.

Longuet-Higgins, M. S., 2005: On wave set-up in shoaling water with a rough sea bed, *Journal of Fluid Mechanics*, **527**, 217-234.

Longuet-Higgins, M. S., and R. W. Stewart, 1962: Radiation Stress and Mass Transport in Gravity Waves, with Application to Surf Beats, *Journal of Fluid Mechanics*, **13**, 481-504.

Lowe, R. J., J. L. Falter, M. D. Bandet, G. Pawlak, M. J. Atkinson, S. G. Monismith and J. R. Koseff, Spectral wave dissipation over a barrier reef, *Journal of Geophysical Research – Oceans*, **110**, C04001, doi:010.1029/2004JC002711.

Lugo-Fernandez, A., H. H. Roberts, and W. J. Wiseman, 2004: Currents, water levels, and mass transport over a modern Caribbean coral reef: Tague Reef, St Croix, USVI, *Continental shelf research*, **24,** 1989-2009.

Lugo-Fernandez, A., H. H. Roberts, W. J. Wiseman, and B. L. Carter, 1998: Water level and currents of tidal and infragravity periods at Tague Reef, St. Croix (USVI), *Coral Reefs*, **17**, 343-349.

PRELIMINARY ACCEPTED VERSION

AMERICAN METEOROLOGICAL SOCIETY 1919

Macmahan, J. H., E. B. Thornton, and A. Reniers, 2006: Rip current review, *Coastal Engineering*, **53**, 191-208.

Massel, S. R., and M. R. Gourlay, 2000: On the modelling of wave breaking and set-up on coral reefs, *Coastal Engineering*, **39**, 1-27.

Mei, C. C., 1989: *The applied dynamics of ocean surface waves*, World Scientific.

Monismith, S. G., 2007: Hydrodynamics of Coral Reefs, *Annual Review of Fluid Mechanics*, **39**, 37-55**.**

Munk, W. H., and M. C. Sargent, 1954: Adjustment of Bikini Atoll to ocean waves, *USGS Professional Paper 260-I*.

Nielsen, P., Guard, P.A., Callaghan, D.P, and T.E. Baldock, 2008: Observations of wave pump efficiency, *Coastal Engineering*, **55**, 69-72.

Pawlowicz, R., B. Beardsley, and S. Lentz, 2002: Classical tidal harmonic analysis including error estimates in MATLAB using TTIDE, *Computers and Geosciences*, **28**, 929-927.

Putrevu, U., J. Oltmanshay, and I. A. Svendsen, 1995: Effect of alongshore nonuniformities on longshore-current predictions, *Journal of Geophysical Research-Oceans*, **100**, 16119-16130.

Raubenheimer, B., R. T. Guza, and S. Elgar, 2001: Field observations of wave-driven setdown and setup, *Journal of Geophysical Research-Oceans*, **106**(C3), 4629-4638.

Reidenbach, M. A., S. G. Monismith, J. R. Koseff, G. Yahel, and A. Genin, 2006: Boundary layer turbulence and flow structure over a fringing coral reef, *Limnology and oceanography*, **51**, 1956-1968.

Reniers, A., and J. A. Battjes, 1997: A laboratory study of longshore currents over barred and non-barred beaches, *Coastal Engineering*, **30**, 1-21.

Roberts, H. H., S. P. Murray, and J. N. Suhayda, 1975: Physical Processes in Fringing Reef System, *Journal of Marine Research*, **33***,* 233-260.

PRELIMINARY ACCEPTED VERSION

Stockdon, H. F., R. A. Holman, P. A. Howd, and A. H. Sallenger, 2006: Empirical parameterization of setup, swash, and runup, *Coastal Engineering*, **53**, 573-588.

Symonds, G., K. P. Black, and I. R. Young, 1995: Wave-Driven Flow over Shallow Reefs, *Journal of Geophysical Research-Oceans*, **100**(C2), 2639-2648.

Tait, R. J., 1972: Wave set-up on coral reefs, *Journal of Geophysical Research*, **77**, 2207-2211.

Thornton, E. B., and R. T. Guza, 1983: Transformation of Wave Height Distribution, *Journal of Geophysical Research-Oceans and Atmospheres*, **88**(C10), 5925-5938.

Thornton, E. B., and C. S. Kim, 1993: Longshore-current and wave height modulation at tidal frequency inside the surf zone, *Journal of Geophysical Research-Oceans*, **98**, 16509-16519.

Warner, J. C., W. R. Geyer, and J. A. Lerczak, 2005: Numerical modeling of an estuary: a comprehensive skill assessment, *Journal of Geophysical Research*, **110**, C05001, doi:10.1029/2004JC002691.

PRELIMINARY ACCEPTED VERSION

AMERICAN METEOROLOGICAL SOCIETY 1919

Table 1. Instrument locations, configurations and deployment information. Two sampling strategies were employed: 1) a long-term (~10-month) deployment at representative sites on the forereef, reef flat, and in the lagoon; and 2) a shorter (~2 month) deployment in winter 2006 where several additional instruments were added to the base array.

Site	Instrument	Depth (m)	Bin size (m)	Conditions measured	Deployment	Duration
A1 (channel)	ADCP (1200kHz)	6.3	0.15	currents	17 January 2006 – 22 March 2006	64
A2 (reef flat)	ADCP (1200kHz)	2.0	0.05	currents, waves	07 June 2005 – 24 March 2006	272
A3 (reef flat)	ADCP (1200kHz)	2.0	0.05	currents, waves	07 June 2005 – 22 March 2006	240
A4 (reef flat)	ADCP (1200kHz)	5.1	0.10	currents, waves	17 January 2006 – 23 March 2006	65
A5 (channel)	ADCP (1200kHz)	11.4	0.30	currents	17 January 2006 – 22 March 2006	64
A6 (lagoon)	ADCP (600kHz)	15.3	0.50	currents	18 January 2006 – 24 March 2006	65
A7 (lagoon)	ADCP (600kHz)	15.8	0.50	currents	18 January 2006 – 23 March 2006	64
W1 (forereef)	SBE 26	8.1	-	waves	07 June 2005 – 22 March 2006	282
W2 (forereef)	SBE 26	7.9	-	waves	15 January 2006 – 22 March 2006	66
W3 (reef flat)	SBE 26	2.7	-	waves	21 January 2006 – 19 March 2006	57
W4 (reef flat)	SBE 26	2.5	-	waves	21 January 2006 – 19 March 2006	57
W5 (lagoon)	SBE 26	2.3	-	water level	29 Sept 2005 – 22 March 2006	167

PRELIMINARY ACCEPTED VERSION

AMERICAN METEOROLOGICAL SOCIETY 1919

Table 2. Root-mean-squared wave heights (H_{rms}, mean and standard deviation), correlation coefficients R_{tide} between H_{rms} and the local tidal depth, as well as R_{wave} between H_{rms} and the offshore wave height $H_{rms,0}$, Stokes drift estimates (U^S, mean and standard deviation), and the median fraction of the local mass flux due to Stokes drift. Italicized correlations are significant to 95%; bold correlations to 99%. *'s denote results based on the entire 10-month record.

Site	H_{rms} [m] mean (SD)	R_{tide}	R_{wave}	U^S [cm s^{-1}] mean (SD)	$\lvert U^S \rvert / \lvert U^E + U^S \rvert$ median
WO	1.62 (0.40)	-0.08	**1.00**	-	-
WO*	1.41 (0.38)	0.12	**1.00**	-	-
W1	1.29 (0.34)	-0.08	**0.90**	3.7 (2.0)	-
W2	1.16 (0.28)	-0.07	**0.89**	3.0 (1.5)	-
W2*	1.01(0.32)	0.16	**0.92**	2.3 (1.7)	-
A1	-	-	-	-	-
A2	0.40 (0.06)	**0.76**	*0.24*	2.9 (0.5)	0.27
A2*	0.36 (0.08)	**0.68**	**0.30**	2.4 (0.8)	0.36
A3	0.43 (0.05)	**0.89**	*0.16*	3.3 (0.4)	0.17
A3*	0.40 (0.07)	**0.72**	**0.32**	3.0 (0.7)	0.21
A4	0.64 (0.11)	**0.33**	**0.67**	1.7 (0.5)	0.25
A5	-	-	-	-	-
W3	0.32 (0.07)	**0.47**	**0.58**	1.0 (0.4)	-
W4	0.45 (0.08)	**0.41**	**0.80**	2.1 (0.7)	-

PRELIMINARY ACCEPTED VERSION

AMERICAN METEOROLOGICAL SOCIETY 1919

Table 3. Depth-averaged Eulerian current statistics, expressed in cm s^{-1}. Time-averaged current vectors and current ellipse axes, with the axes values representing one standard deviation of the variability. Magnitude of the tidal current amplitude for the M2 component inferred via harmonic analysis. R_{tide} defined as the square-root of the total current variability explained by the harmonic analysis. Correlation coefficient R_{wave} of the subtidal (38-hour low pass filtered) current (positive into the bay) with the offshore rms wave height $H_{rms,0}$. Threshold rms wave height H_r inferred from subtidal currents. Italicized correlations are significant to 95%; bold-italicized correlations to 99%. *'s denote results based on the entire 10-month record.

	Average Eulerian current		Principal component axes			M2 current			
Site	Magnitude	Direction	Major	Minor	Orientation	amplitude	R_{tide}	R_{wave}	H_r [m]
A1	11.5	40	10.0	1.6	39	7.1	**0.61**	**-0.93**	0.8±0.1
A2	9.0	230	6.4	3.5	246	1.9	*0.26*	**0.85**	0.7±0.1
A2*	5.4	231	6.0	3.3	245	2.0	**0.28**	**0.84**	0.7±0.1
A3	17.1	275	8.9	1.8	264	1.9	*0.26*	**0.91**	0.6±0.1
A3*	12.6	280	8.7	1.9	267	2.1	**0.29**	**0.94**	0.6±0.1
A4	5.6	343	4.1	2.3	336	2.0	**0.48**	**0.88**	0.7±0.1
A5	8.7	44	9.5	1.1	43	4.2	**0.56**	**-0.81**	0.8±0.1
A6	0.7	147	4.5	0.7	146	3.8	**0.81**	*0.22*	-
A7	1.5	9	6.6	0.8	357	4.1	**0.71**	*-0.31*	-

PRELIMINARY ACCEPTED VERSION

Table 4. Wave setup scaling. Nonlinear regression coefficients *m* and *n* based on a fit governed by $\bar{\eta} = aH_{rms,0}^{m}T_p^{n} - b$ [(15)], and the coefficient of determination for the best fit (R^2). Setup estimated from the regression coefficients for $H_{rms,0} = 2$ m with $T_p = 7$ s. Uncertainties represent the 95% confidence intervals for the nonlinear least squares parameter estimates. *'s denote results based on the entire 10-month record.

	Site	*m*	*n*	R^2	$\bar{\eta}$ [cm]
A2	(reef flat)	1.8±0.4	0.8±0.2	0.96	7.7±3.8
A2*	(reef flat)	2.3±0.2	1.0±0.2	0.90	7.9±3.5
A3	(reef flat)	2.0±0.4	0.7±0.2	0.96	5.6±2.3
A3*	(reef flat)	2.4±0.3	0.9±0.2	0.93	5.9±2.0
A4	(reef flat)	2.9±0.7	0.7±0.4	0.88	4.0±2.2
W3	(back reef)	2.8±0.8	0.7±0.4	0.87	3.9±2.1
W4	(back reef)	2.3±0.7	0.6±0.4	0.86	3.6±2.0
W5	(lagoon)	2.3±0.6	0.7±0.4	0.86	4.3±1.9
W5*	(lagoon)	2.4±0.4	0.8±0.3	0.85	4.4±1.7

PRELIMINARY ACCEPTED VERSION

AMERICAN METEOROLOGICAL SOCIETY 1919

Table 5. Reef geometry parameters, and estimated quadratic ($C_{D,r}$, $C_{D,c}$) and linear ($C'_{D,r}$, $C'_{D,c}$) drag coefficients derived for the reef and lagoon-channel regions, respectively. Values are shown for each of the two dominant circulation cells (southern and northern). Uncertainties denote the 95% confidence intervals of the parameter estimates.

	W_{total} (m)	W_r / W_{total}	$C_{D,r}$	$C_{D,c}$	$C'_{D,r}$	$C'_{D,c}$
South cell	2300±400	0.71±0.16	0.031±0.019	0.015±0.009	0.023±0.013	0.014±0.009
North cell	3800±400	0.73±0.13	0.011±0.006	0.009±0.006	0.013±0.007	0.008±0.005

PRELIMINARY ACCEPTED VERSION

AMERICAN METEOROLOGICAL SOCIETY 1919

Figure captions

Figure 1. a) An idealized cross-shore reef transect having the following distinctive features: a sloping forereef, a shallow reef flat and a relatively deep lagoon. The dominant momentum terms (equations) are shown, with the surfzone represented as a transition zone. Wave breaking on the forereef causes wave setup (dashed line) that drives a cross-reef flow towards a deeper lagoon. For lagoons bounded by a coastline (not shown), the flow returns to the ocean via reef channels (also not shown). Note that the vertical scales of the bathymetry and wave setup are both highly exaggerated. b) Plan view of an idealized reef-lagoon-channel system bounded by a shoreline, denoting the distinct reef (below the dashed line) and channel regions (above the dashed line). Flow moves from points A through D.

Figure 2. Kaneohe Bay, Oahu, Hawaii. a) Quickbird aerial photograph (© Digitalglobe) with the instrument locations superimposed. The offshore wave buoy (not shown) is located ~8 km southeast of Mokapu peninsula bounding the southern end of the bay. b) The bathymetry, highlighting its dominant morphological features.

Figure 3. Physical forcing conditions during the winter experiment. a) Tidal elevation. b) Offshore rms wave height $H_{rms,0}$ measured by the offshore wave buoy (WO). c) Offshore peak wave period T_p. d) Offshore mean wave direction θ_m (note that 45^o is the shore-normal direction).

Figure 4. a) Time-series of rms wave height H_{rms} measured on the forereef (site W1) and reef flat (site A2) during the winter experiment, based on raw (non-subtidally filtered) data. b) Local wave height versus local water depth on the forereef at site W1. c) Local wave height versus local water depth on the reef flat at site A2. The dashed line represents the depth-limited maximum wave height $H_{rms,\max} = \gamma_r h_r$ with $\gamma_r = 0.3$, above which waves were not observed.

PRELIMINARY ACCEPTED VERSION

AMERICAN METEOROLOGICAL SOCIETY 1919

Figure 5. a) Time-averaged Eulerian current vectors, b) principle component ellipses (radii represent one current velocity standard deviation), c) time-averaged Stokes drift vectors, and d) M2 tidal ellipses. All data is from the winter (~ 2 month) deployment and based on the total flow variability (i.e., non-subtidally filtered). Note the differences in the velocity scales between the figures.

Figure 6. Subtidal Eulerian current speeds U^E along the principal major axis, measured at the a) reef flat (site A2), b) channel (site A1), and c) lagoon (site A7), as a function of the rms offshore wave height $H_{rms,0}$.

Figure 7. a) Time series of subtidal Eulerian velocity U^E and subtidal Stokes drift velocity U^S, along the principal major axis at A2.

Figure 8. a) Time-series of subtidal variability in wave setup $\bar{\eta}$ measured on the reef flat (A2) and in the lagoon (W5), during the winter deployment. Wave setup versus $H_{rms,0}^2 T_p$ plotted for the entire 10-month experiment, as measured on b) the reef flat (A2) and c) inside the lagoon (W5).

Figure 9. Linear regression ($y = Ax$) used to estimate an effective reef width W_r for the two circulation cells. Note that a zero y-intercept was assumed in order to satisfy **(7)**. a) South (Sampan channel) cell using the depth-averaged transport (Eulerian plus Stokes drift) at reef A2 and channel A1 sites (R^2=0.78). b) North (Ship channel) cell using the depth-averaged transport at reef A3 and channel A5 sites (R^2=0.56). Solid gray lines represent the best linear fit to the data; dashed lines bound the 95% confidence limits of the line of best fit.

Figure 10. Linear regression ($y = Ax$) of subtidal water level differences versus Eulerian current speeds squared, used to infer quadratic drag coefficients. a) Water level difference between A2 and W5 versus the reef current squared at A2 (R^2=0.57). b) Water level difference between A3 and

PRELIMINARY ACCEPTED VERSION

W5 versus the reef current squared at A3 (R^2=0.34). c) Water level difference between W5 and the channel exit (where $\bar{\eta}$ is assumed to be zero), versus the channel current squared at A1 (R^2=0.70). d) Water level difference between W5 and the channel exit, versus the channel current squared at A5 (R^2=0.63). Solid gray lines represent the best linear fits to the data; dashed lines bound the 95% confidence limits of the lines of best fit.

Figure 11. Model results across the reef obtained using TG83 (with and without wave friction), applied to the southern circulation cell for $H_{rms,0} = 2$ m, $T_p = 7$ s (note the lagoon-channel region is not shown). Squares are derived from field data, based on representative values when $H_{rms,0} = 2$ m (i.e., based on the regression coefficient in Table 4 for setup). Error bars are derived from uncertainties in the regression coefficients. For comparison, predictions from H99 and GC05 ($K_p = 0.2$) are also included. a) Assumed cross-shore depth profile; b) wave height distribution H_{rms}; c) setup distribution $\bar{\eta}$; d) depth-average Eulerian current speed U^E; and e) depth-averaged Stokes drift speed U^S. Note that the H99 model is applied using the same parameters recommended in that paper (i.e., using different γ's on the forereef and reef flat), except we use a slightly smaller $\gamma_r = 0.3$ to reflect the observed reef flat wave heights (see Figure 4). The TG83 model is applied with the identical parameter values used in Lowe et al. (2005).

Figure 12. Time-series of field observations and model predictions using TG83 (including wave friction), during the winter experiment period, of: a) reef-top setup $\bar{\eta}_r$ (at A2), b) lagoon setup $\bar{\eta}_L$ (at W5) and c) Eulerian current speed U_r^E (at A2). Model predictions are shown for both quadratic friction ($C_D = 0.02$) and linear friction ($C_D^L = 0.02$), based on a representative near-bed wave orbital velocity $U_w = 0.2$ m s^{-1}. Model skill values (i.e., calculated via Warner et al. 2005) were: 0.94 (quadratic) and 0.94 (linear) for $\bar{\eta}_r$; 0.90 (quadratic) and 0.86 (linear) for $\bar{\eta}_L$; and 0.84

PRELIMINARY ACCEPTED VERSION

(quadratic) and 0.90 (linear) for U_r^E. Perfect agreement will yield a skill of one, whereas complete disagreement will yield a skill of zero. Corresponding R^2 values were: 0.94 (quadratic) and 0.94 (linear) for $\bar{\eta}_r$; 0.82 (quadratic) and 0.81 (linear) for $\bar{\eta}_L$; and 0.80 (quadratic) and 0.78 (linear) for U_r^E.

Figure 13. Effect of varying lagoon-channel dimensions on a) setup distribution $\bar{\eta}$, and b) cross-reef Eulerian current U^E speed for $H_{rms,0} = 2$ m, T=7 s. The model is applied using the same reef dimensions for Kaneohe Bay used in Figure 11 (L_r, h_r, W_r, forereef slope) and a fixed channel width W_c with $C_D = 0.02$. The return path length L_c is also held fixed and the lagoon-channel depth h_c is varied. Note that for small h_c / L_c, U^E on the forereef (x<0) is directed offshore to offset the relatively strong Stokes drift in this region, i.e. to conserve the total mass flux q across the reef.

PRELIMINARY ACCEPTED VERSION

AMERICAN METEOROLOGICAL SOCIETY 1919

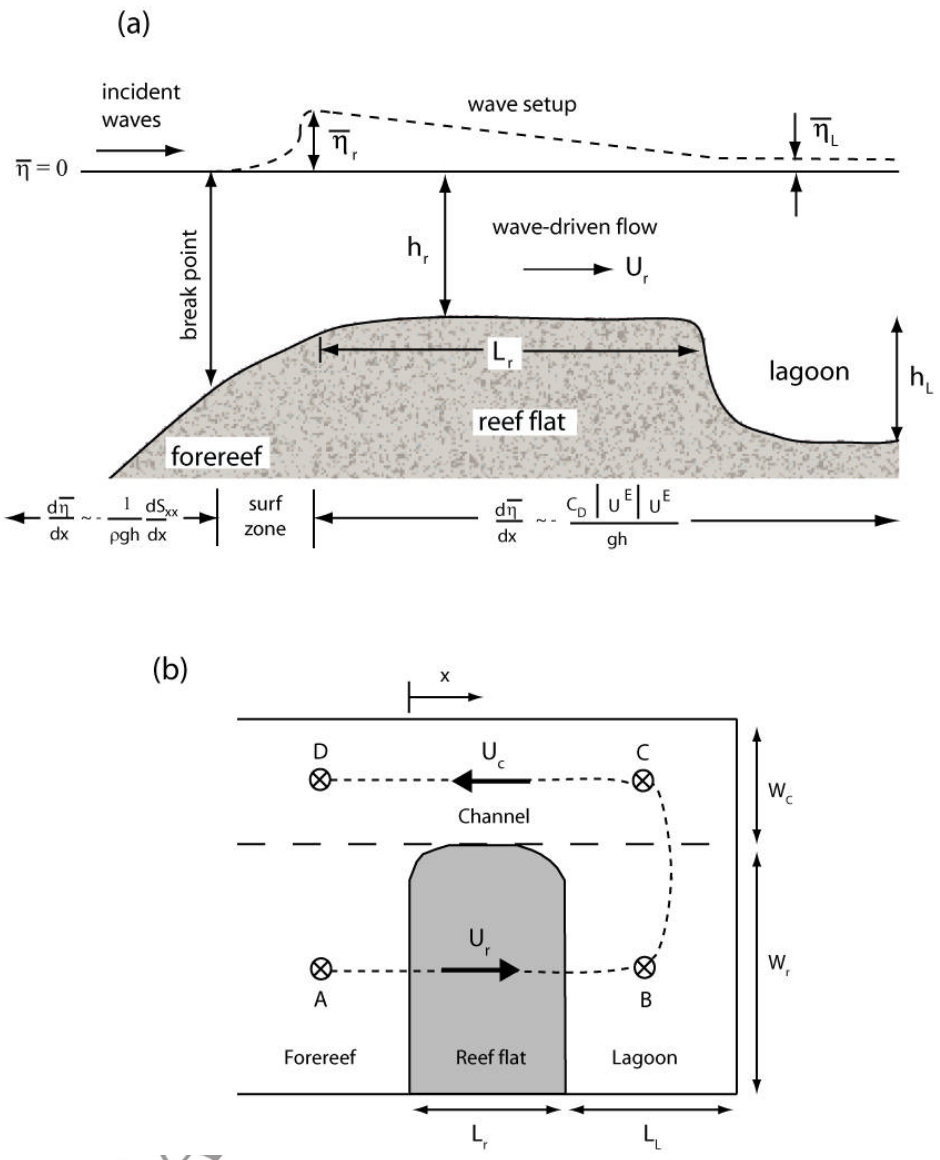

Figure 1. a) An idealized cross-shore reef transect having the following distinctive features: a sloping forereef, a shallow reef flat and a relatively deep lagoon. The dominant momentum terms (equations) are shown, with the surfzone represented as a transition zone. Wave breaking on the forereef causes wave setup (dashed line) that drives a cross-reef flow towards a deeper lagoon. For lagoons bounded by a coastline (not shown), the flow returns to the ocean via reef channels (also not shown). Note that the vertical scales of the bathymetry and wave setup are both highly exaggerated. b) Plan view of an idealized reef-lagoon-channel system bounded by a shoreline, denoting the distinct reef (below the dashed line) and channel regions (above the dashed line). Flow moves from points A through D.

PRELIMINARY VERSION

AMERICAN METEOROLOGICAL SOCIETY 1919

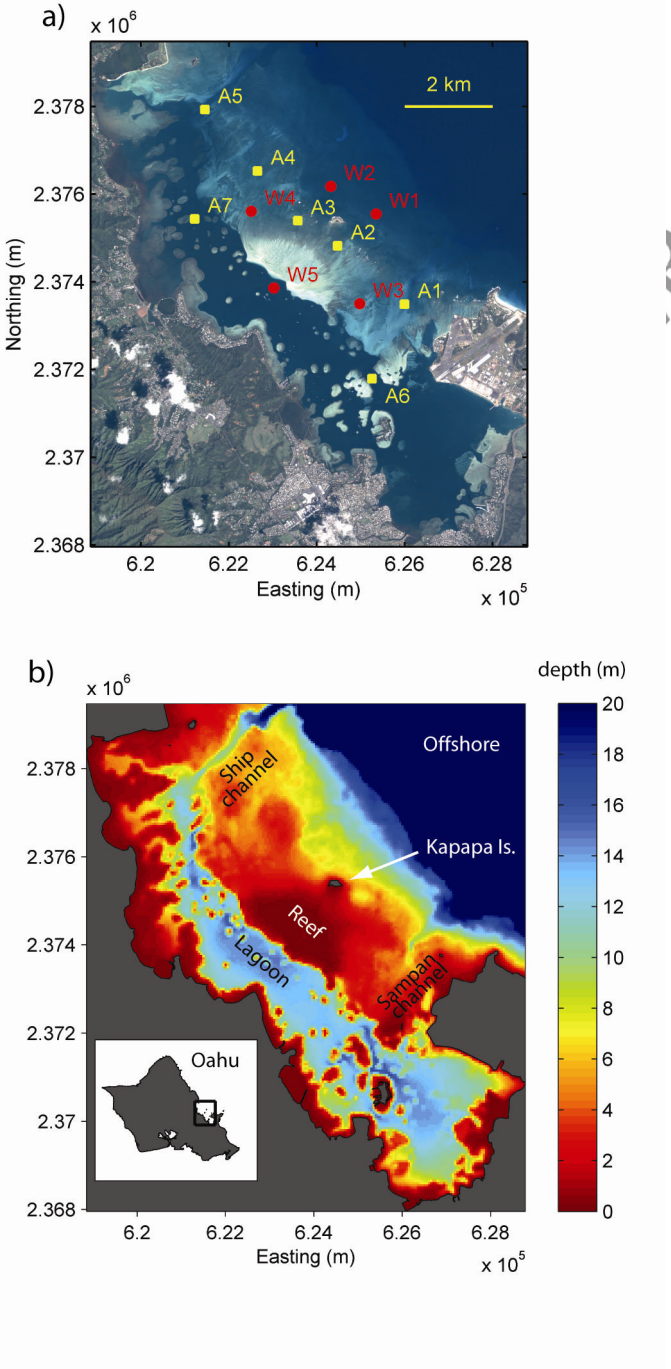

Figure 2. Kaneohe Bay, Oahu, Hawaii. a) Quickbird aerial photograph (© Digitalglobe) with the instrument locations superimposed. The offshore wave buoy (not shown) is located ~8 km southeast of Mokapu peninsula bounding the southern end of the bay. b) The bathymetry, highlighting its dominant morphological features.

PRELIMINARY VERSION

AMERICAN METEOROLOGICAL SOCIETY 1919

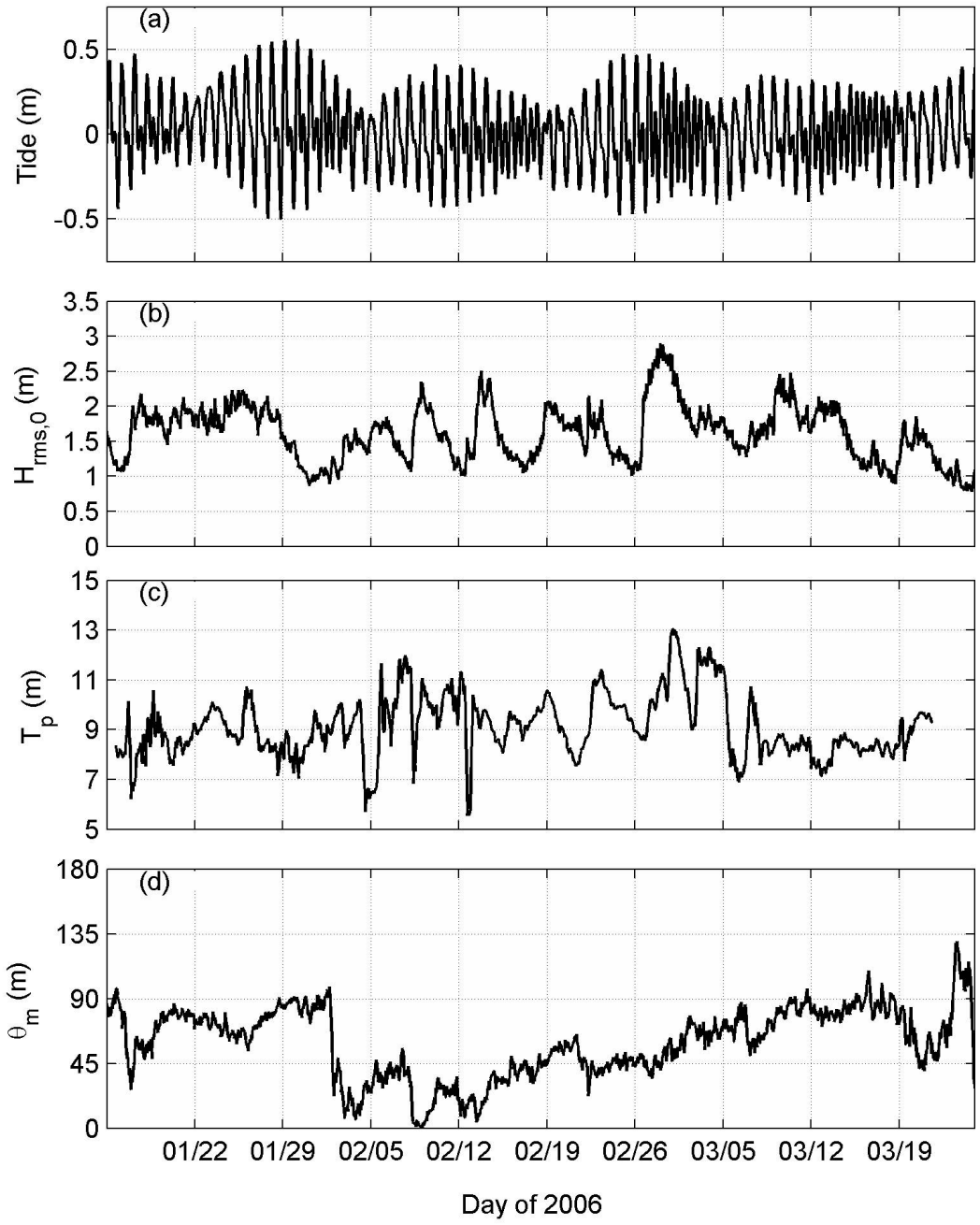

Figure 3. Physical forcing conditions during the winter experiment. a) Tidal elevation. b) Offshore rms wave height $H_{rms,0}$ measured by the offshore wave buoy (WO). c) Offshore peak wave period T_p. d) Offshore mean wave direction θ_m (note that 45^o is the shore-normal direction).

PRELI

AMERICAN METEOROLOGICAL SOCIETY 1919

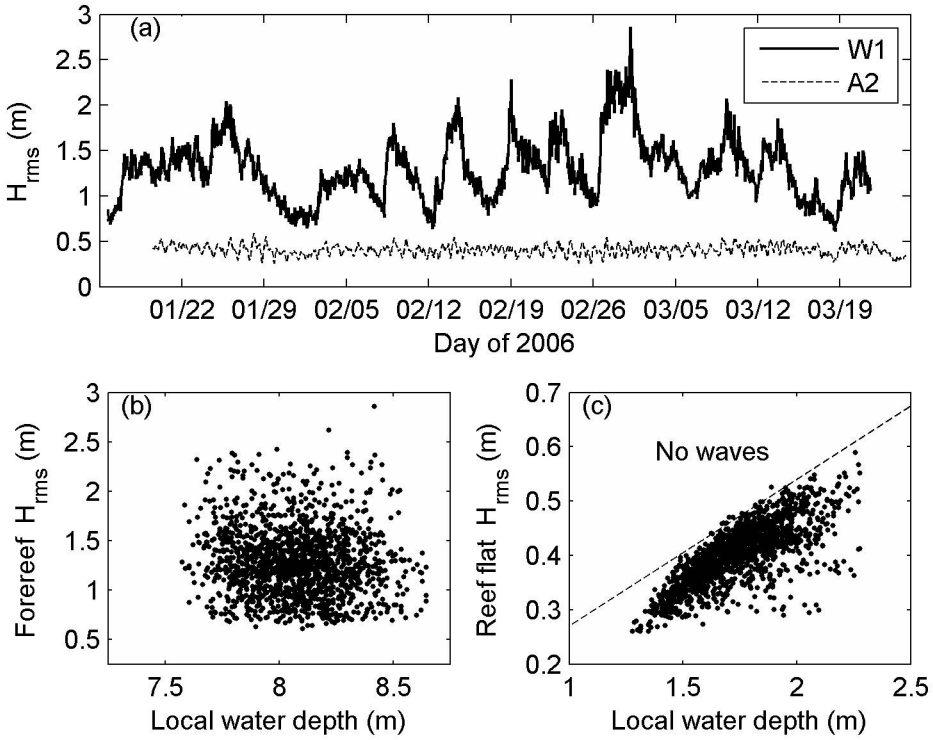

Figure 4. a) Time-series of rms wave height H_{rms} measured on the forereef (site W1) and reef flat (site A2) during the winter experiment, based on raw (non-subtidally filtered) data. b) Local wave height versus local water depth on the forereef at site W1. c) Local wave height versus local water depth on the reef flat at site A2. The dashed line represents the depth-limited maximum wave height $H_{rms,\max} = \gamma_r h_r$ with $\gamma_r = 0.3$, above which waves were not observed.

PRELIMINARY

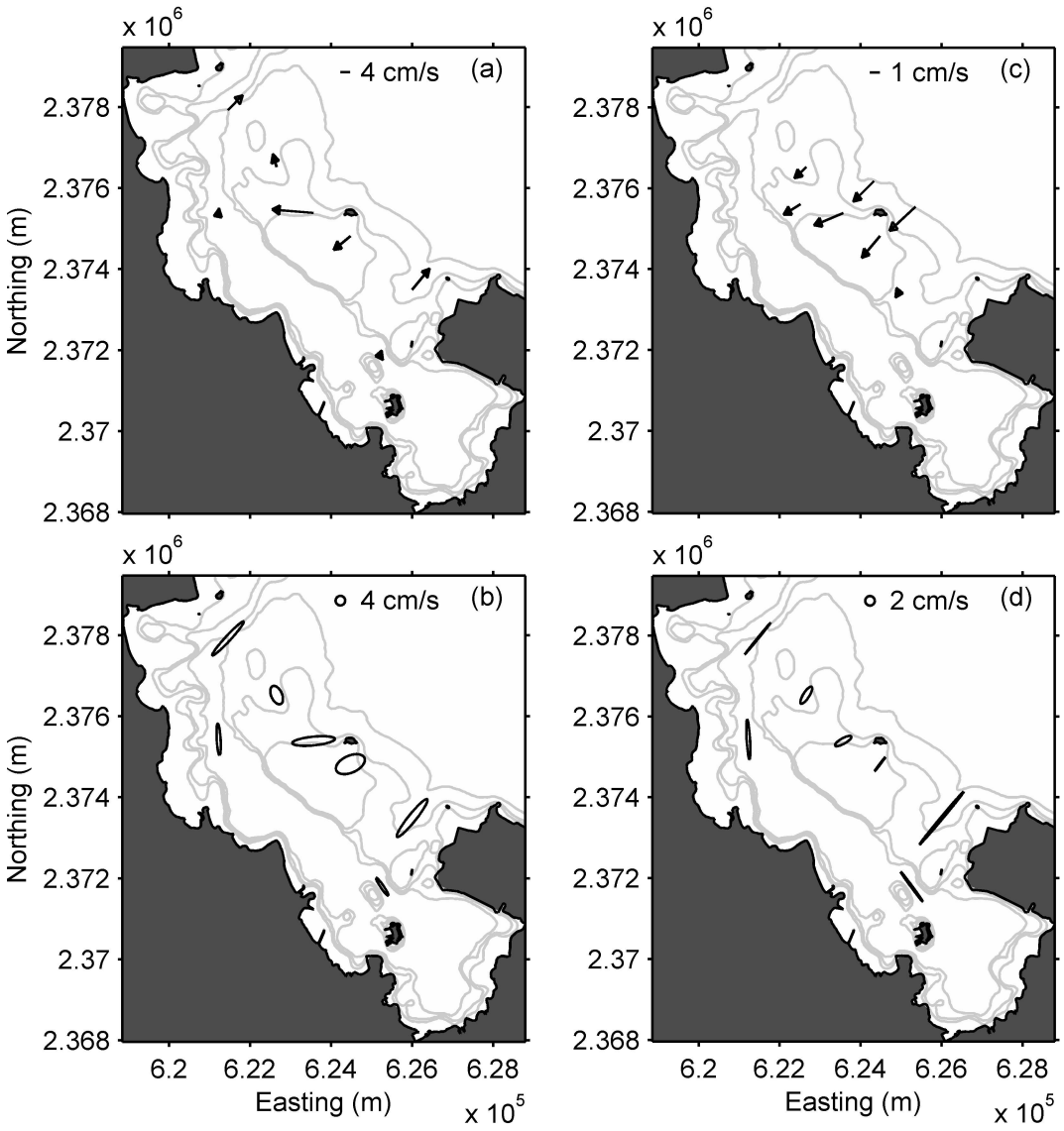

Figure 5. a) Time-averaged Eulerian current vectors, b) principle component ellipses (radii represent one current velocity standard deviation), c) time-averaged Stokes drift vectors, and d) M2 tidal ellipses. All data is from the winter (~ 2 month) deployment and based on the total flow variability (i.e., non-subtidally filtered). Note the differences in the velocity scales between the figures.

PRELIMINARY

AMERICAN METEOROLOGICAL SOCIETY 1919

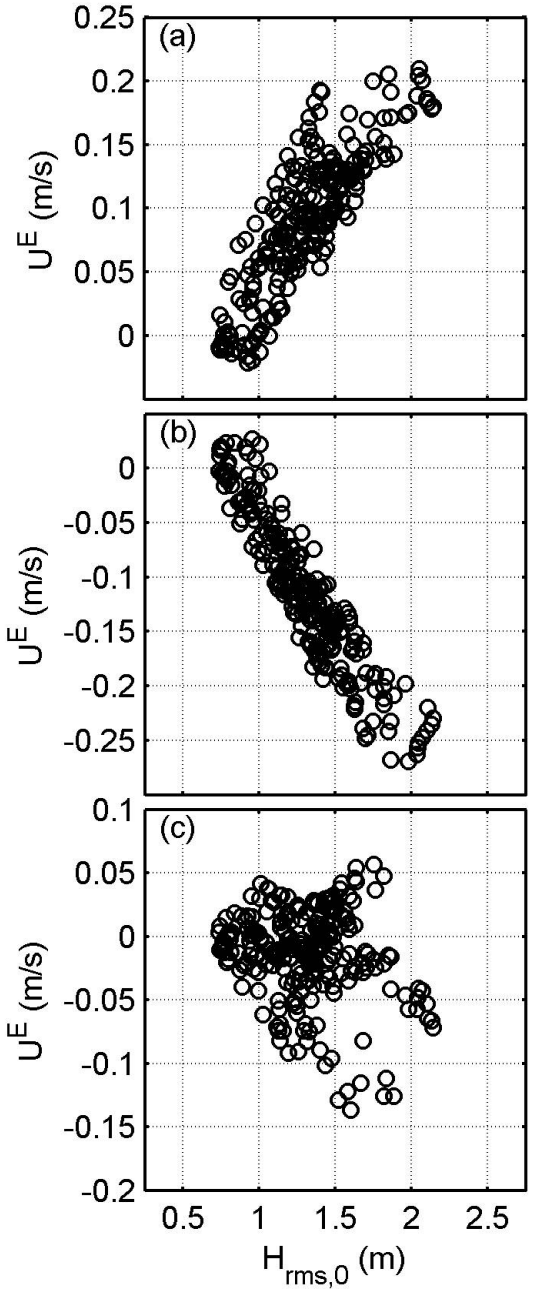

Figure 6. Subtidal Eulerian current speeds U^E along the principal major axis, measured at the a) reef flat (site A2), b) channel (site A1), and c) lagoon (site A7), as a function of the rms offshore wave height $H_{rms,0}$.

PRELIMINARY VERSION

AMERICAN METEOROLOGICAL SOCIETY 1919

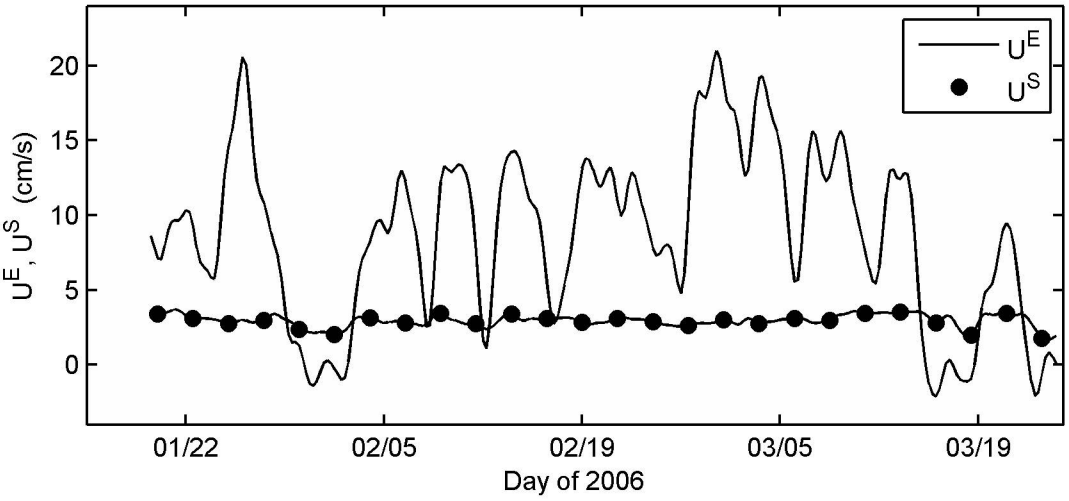

Figure 7. a) Time series of subtidal Eulerian velocity U^E and subtidal Stokes drift velocity U^S, along the principal major axis at A2.

PRELIMINARY ACCEPT

AMERICAN METEOROLOGICAL SOCIETY 1919

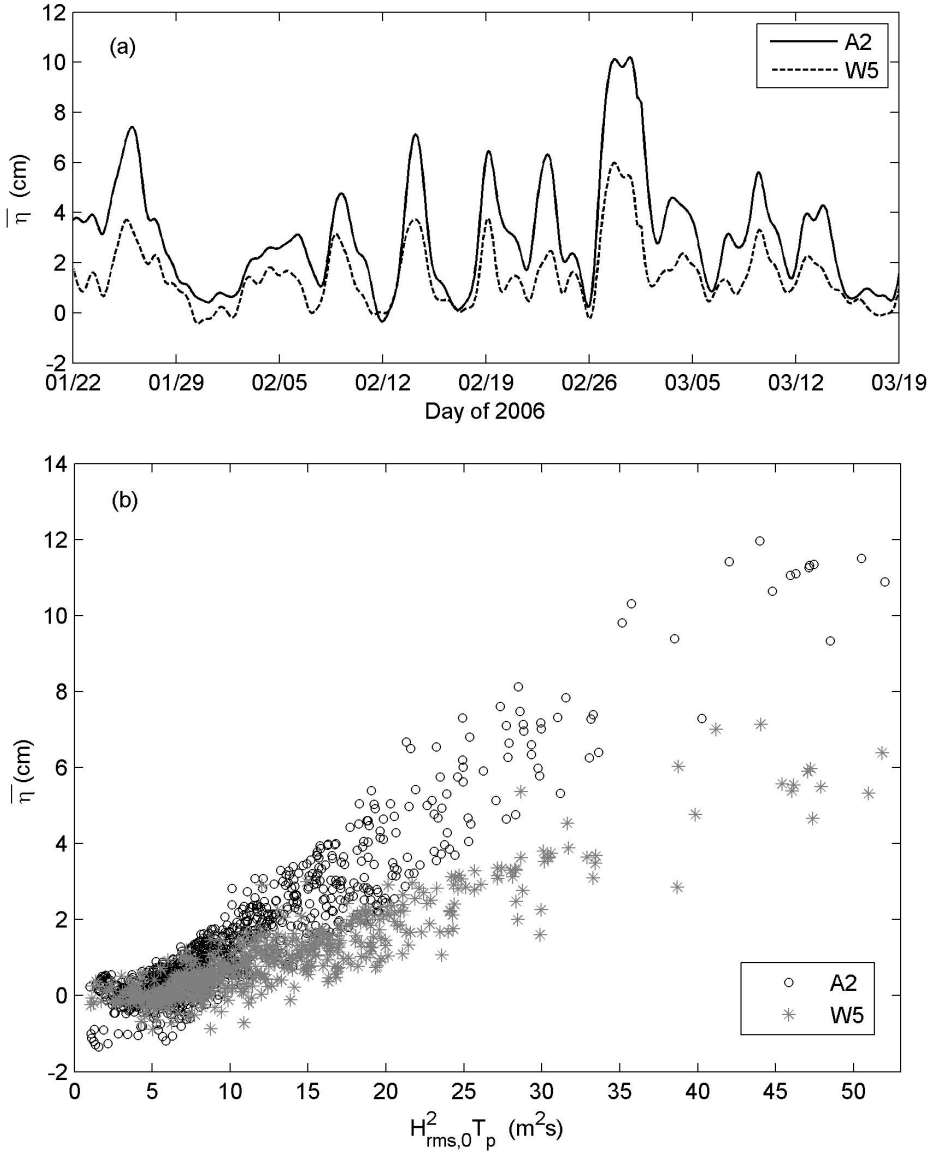

Figure 8. a) Time-series of subtidal variability in wave setup $\overline{\eta}$ measured on the reef flat (A2) and in the lagoon (W5), during the winter deployment. Wave setup versus $H^2_{rms,0}T_p$ plotted for the entire 10-month experiment, as measured on b) the reef flat (A2) and c) inside the lagoon (W5).

PRELIM

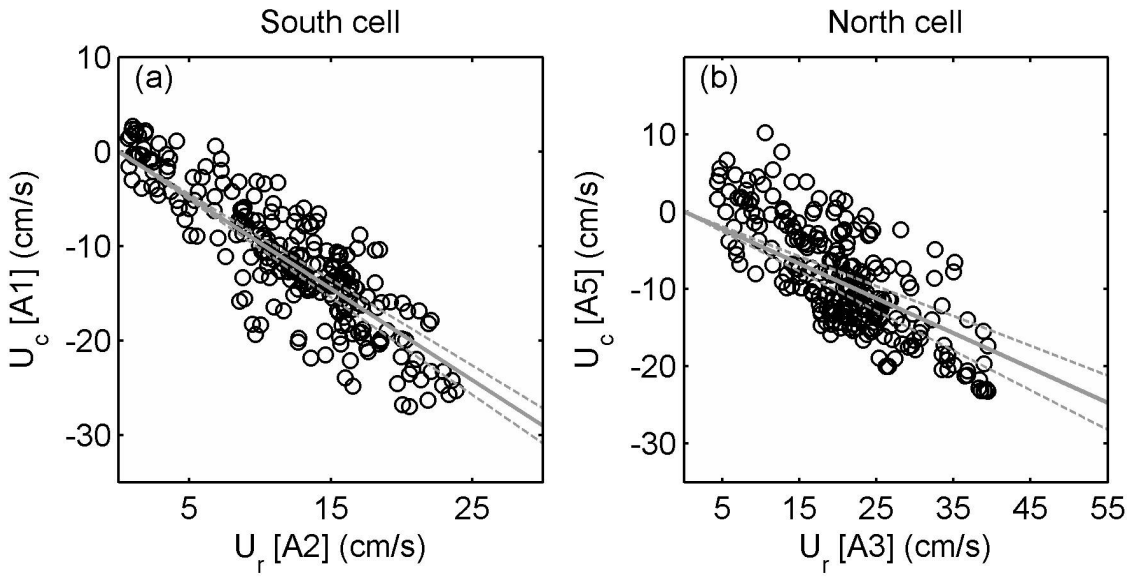

Figure 9. Linear regression ($y = Ax$) used to estimate an effective reef width W_r for the two circulation cells. Note that a zero *y*-intercept was assumed in order to satisfy (7). a) South (Sampan channel) cell using the depth-averaged transport (Eulerian plus Stokes drift) at reef A2 and channel A1 sites (R^2=0.78). b) North (Ship channel) cell using the depth-averaged transport at reef A3 and channel A5 sites (R^2=0.56). Solid gray lines represent the best linear fit to the data; dashed lines bound the 95% confidence limits of the line of best fit.

PRELIMINARY ACCEPTED

AMERICAN METEOROLOGICAL SOCIETY 1919

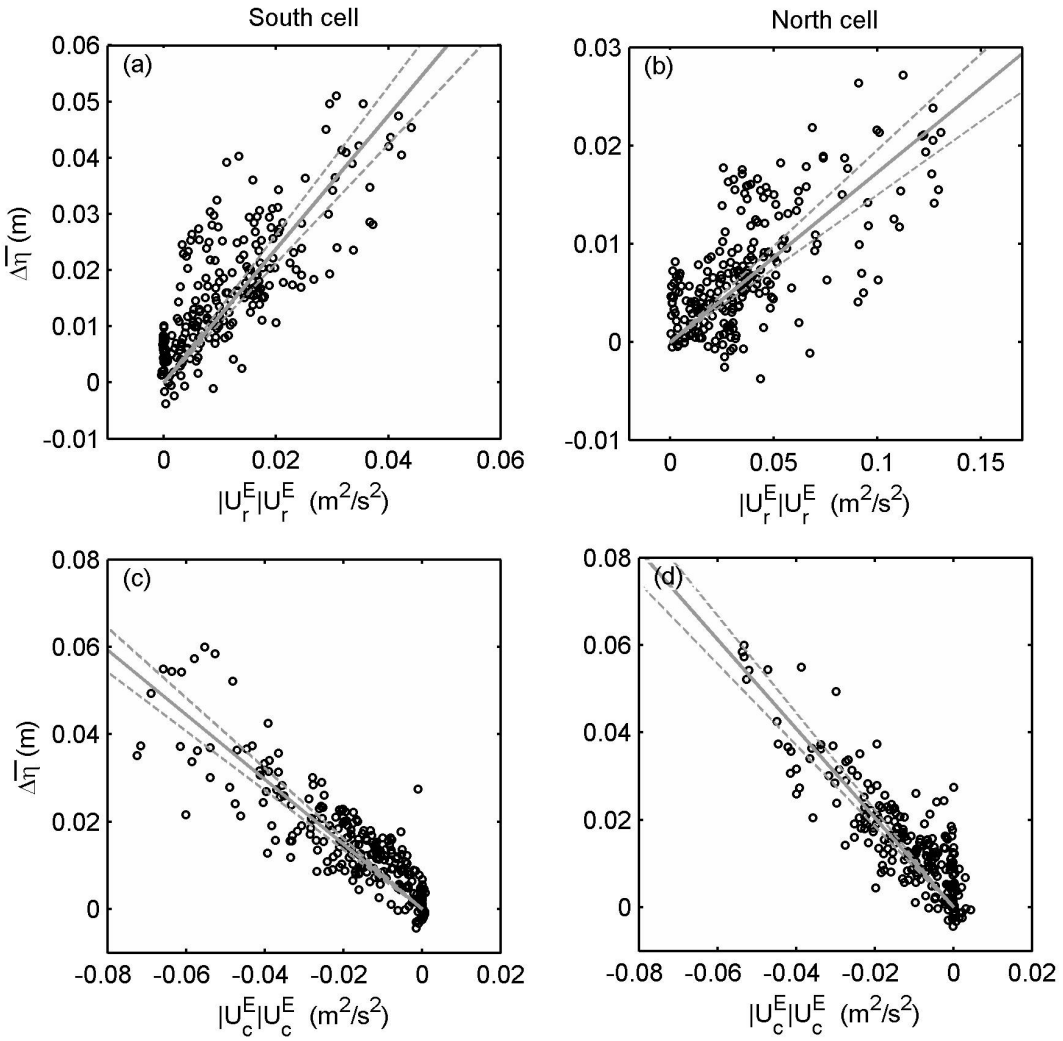

Figure 10. Linear regression ($y = Ax$) of subtidal water level differences versus Eulerian current speeds squared, used to infer quadratic drag coefficients. a) Water level difference between A2 and W5 versus the reef current squared at A2 (R^2=0.57). b) Water level difference between A3 and W5 versus the reef current squared at A3 (R^2=0.34). c) Water level difference between W5 and the channel exit (where $\overline{\eta}$ is assumed to be zero), versus the channel current squared at A1 (R^2=0.70). d) Water level difference between W5 and the channel exit, versus the channel current squared at A5 (R^2=0.63). Solid gray lines represent the best linear fits to the data; dashed lines bound the 95% confidence limits of the lines of best fit.

PRELIMINARY

AMERICAN METEOROLOGICAL SOCIETY 1919

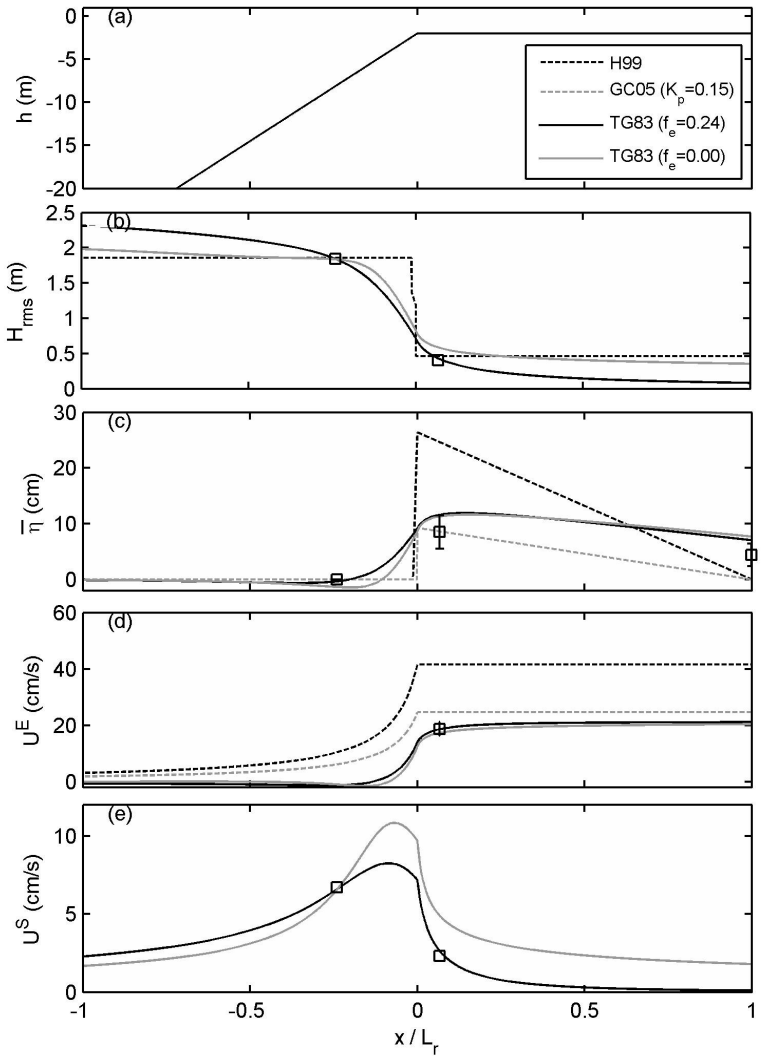

Figure 11. Model results across the reef obtained using TG83 (with and without wave friction), applied to the southern circulation cell for $H_{rms,0} = 2$ m, $T_p = 7$ s (note the lagoon-channel region is not shown). Squares are derived from field data, based on representative values when $H_{rms,0} = 2$ m (i.e., based on the regression coefficient in Table 4 for setup). Error bars are derived from uncertainties in the regression coefficients. For comparison, predictions from H99 and GC05 ($K_p = 0.2$) are also included. a) Assumed cross-shore depth profile; b) wave height distribution H_{rms}; c) setup distribution $\overline{\eta}$; d) depth-average Eulerian current speed U^E; and e) depth-averaged Stokes drift speed U^S. Note that the H99 model is applied using the same parameters recommended in that paper (i.e., using different γ's on the forereef and reef flat), except we use a slightly smaller $\gamma_r = 0.3$ to reflect the observed reef flat wave heights (see Figure 4). The TG83 model is applied with the identical parameter values used in Lowe et al. (2005).

PRELIMINARY

AMERICAN METEOROLOGICAL SOCIETY 1919

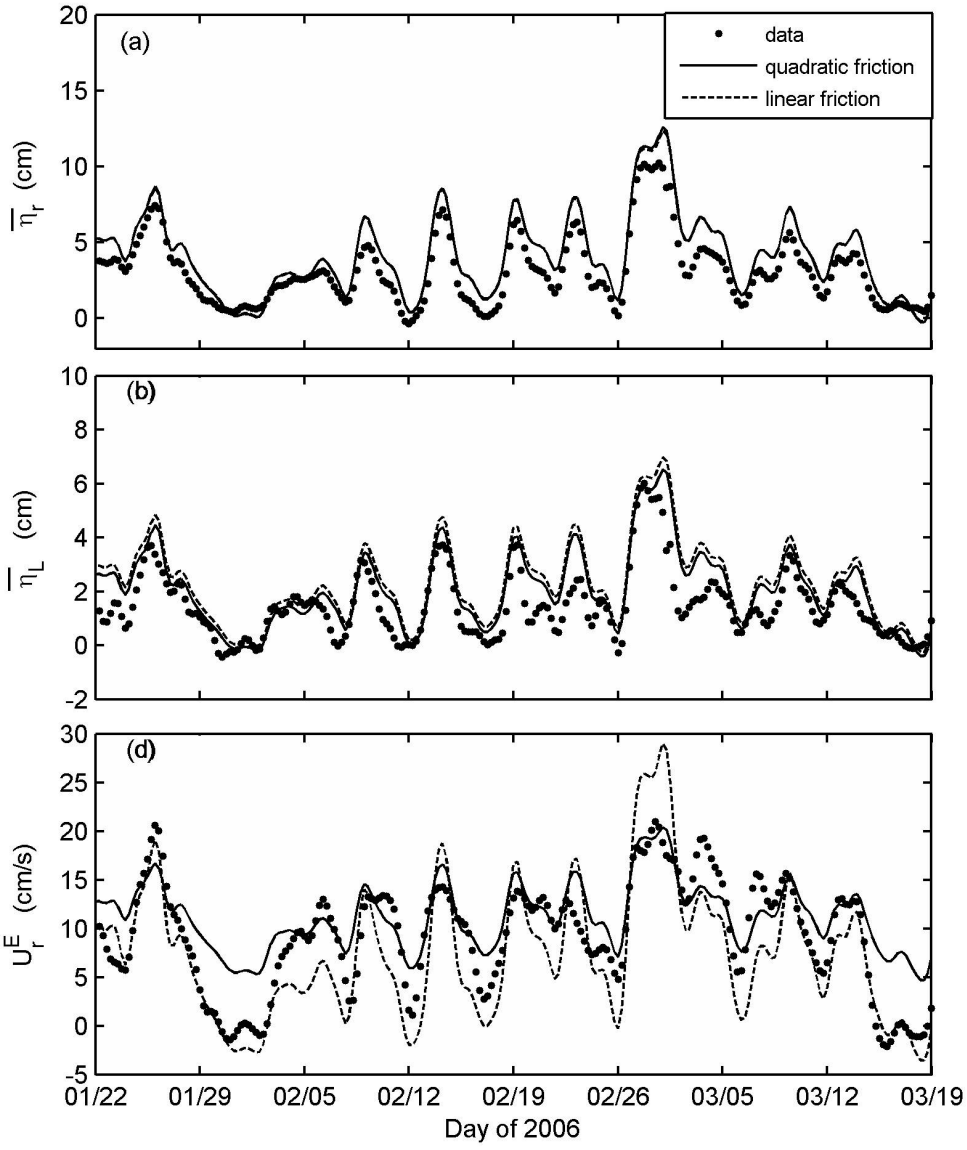

Figure 12. Time-series of field observations and model predictions using TG83 (including wave friction), during the winter experiment period, of: a) reef-top setup $\overline{\eta}_r$ (at A2), b) lagoon setup $\overline{\eta}_L$ (at W5) and c) Eulerian current speed U_r^E (at A2). Model predictions are shown for both quadratic friction ($C_D = 0.02$) and linear friction ($C_D^L = 0.02$), based on a representative near-bed wave orbital velocity $U_w = 0.2$ m s^{-1}. Model skill values (i.e., calculated via Warner et al. 2005) were: 0.94 (quadratic) and 0.94 (linear) for $\overline{\eta}_r$; 0.90 (quadratic) and 0.86 (linear) for $\overline{\eta}_L$; and 0.84 (quadratic) and 0.90 (linear) for U_r^E. Perfect agreement will yield a skill of one, whereas complete disagreement will yield a skill of zero. Corresponding R^2 values were: 0.94 (quadratic) and 0.94 (linear) for $\overline{\eta}_r$; 0.82 (quadratic) and 0.81 (linear) for $\overline{\eta}_L$; and 0.80 (quadratic) and 0.78 (linear) for U_r^E.

PRELIMINARY

AMERICAN METEOROLOGICAL SOCIETY 1919

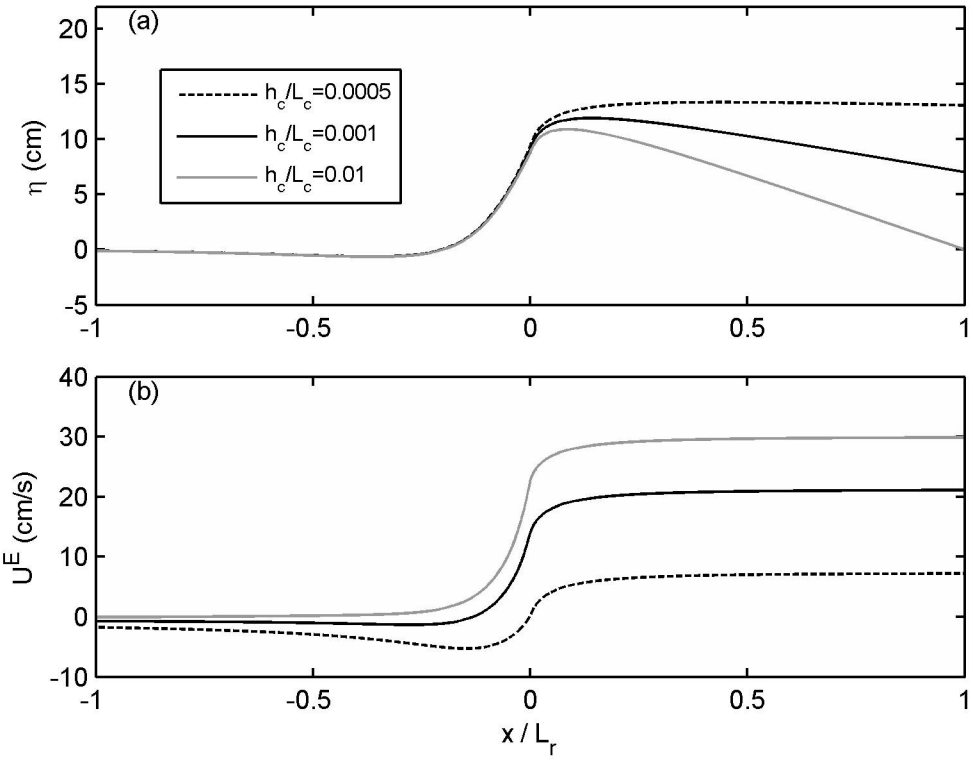

Figure 13. Effect of varying lagoon-channel dimensions on a) setup distribution $\bar{\eta}$, and b) cross-reef Eulerian current U^E speed for $H_{rms,0} = 2$ m, T=7 s. The model is applied using the same reef dimensions for Kaneohe Bay used in Figure 11 (L_r, h_r, W_r, forereef slope) and a fixed channel width W_c with $C_D = 0.02$. The return path length L_c is also held fixed and the lagoon-channel depth h_c is varied. Note that for small h_c / L_c, U^E on the forereef (x<0) is directed offshore to offset the relatively strong Stokes drift in this region, i.e. to conserve the total mass flux q across the reef.

PRELIMINARY ACC